Journal of Zhejiang University-SCIENCE A (Applied Physics & Engineering)
ISSN 1673-565X (Print); ISSN 1862-1775 (Online)
www.jzus.zju.edu.cn; www.springerlink.com
E-mail: jzus@zju.edu.cn

Efficient WENOCU4 scheme with three different adaptive switches*

Liang LI, Hong-bo WANG†‡, Guo-yan ZHAO†‡, Ming-bo SUN, Da-peng XIONG, Tao TANG

Science and Technology on Scramjet Laboratory, National University of Defense Technology, Changsha 410073, China

†E-mail: whbwatch@nudt.edu.cn; zhaoguoyan09@nudt.edu.cn

Received Jan. 19, 2020; Revision accepted June 22, 2020; Crosschecked July 15, 2020

Abstract: Although classical WENOCU schemes can achieve high-order accuracy by introducing a moderate constant parameter C to increase the contribution of optimal weights, they exhibit distinct numerical dissipation in smooth regions. This study presents an extension of our previous research which confirmed that adaptively adjusting parameter C can indeed overcome the inadequacy of the usage of a constant small value. $C_{\min}$ is applied near a discontinuity while $C_{\max}$ is used elsewhere and they are switched according to the variation of the local flow-field property. This study provides the reference values of the adaptive parameter C of WENOCU4 and systematically evaluates the comprehensive performance of three different switches (labeled as the binary, continuous, and hyperbolic tangent switches, respectively) based on an optimized efficient WENOCU4 scheme (labeled as EWENOCU4). Varieties of 1D scalar equations, empirical dispersion relation analysis, and multi-dimensional benchmark cases of Euler equations are analyzed. Generally, the dissipation and dispersion properties of these three switches are similar. Especially, employing the binary switch, EWENOCU4 achieves the best comprehensive properties. Specifically, the binary switch can efficiently filter more misidentifications in smooth regions than others do, particularly for the cases of 1D scalar equations and Euler equations. Also, the computational efficiency of the binary switch is superior to that of the hyperbolic tangent switch. Moreover, the optimized scheme exhibits high-resolution spectral properties in the wavenumber space. Therefore, employing the binary switch is a more cost-effective improvement for schemes and is particularly suitable for the simulation of complex shock/turbulence interaction. This study provides useful guidance for the reference values of parameter C and the evaluation of adaptive switches.

Key words: WENOCU4; Shock-capturing schemes; Adaptive switch; Numerical robustness; Dissipation
https://doi.org/10.1631/jzus.A2000006 **CLC number:** O354.4; O354.5

1 Introduction

Excellent numerical schemes have been developed for the simulation of complex shock/turbulence interaction, and they are simultaneously capable of capturing discontinuities stably and of resolving complex small-scale smooth structures accurately. Nevertheless, it is a great challenge to balance adequate numerical dissipation for stable shock-capturing capacity and a low-dissipation property for resolving small-scale vortical features and simultaneously to maintain superior computational efficiency (Pirozzoli, 2011). Weighted essentially non-oscillatory (WENO) schemes have emerged as one class of the representative and extensively applied shock-capturing schemes proposed for solving Gibbs oscillation problems (Liu et al., 1994; Jiang and Shu, 1996). However, while capturing sharp shock profiles and

‡ Corresponding author

* Project supported by the National Natural Science Foundation of China (Nos. 11522222, 11925207, and 11472305), the Scientific Research Plan of National University of Defense Technology in 2019 (No. ZK19-02), and the Postgraduate Scientific Research Innovation Project of Hunan Province (Nos. CX20200008 and CX20200084), China

ORCID: Liang LI, https://orcid.org/0000-0002-8116-0668; Hong-bo WANG, https://orcid.org/0000-0002-9177-0582; Guo-yan ZHAO, https://orcid.org/0000-0001-7831-7049

free from non-physical oscillations, WENO schemes exhibit obvious numerical dissipation, especially for accurately resolving vortices in the regions with large shear rates or density variation (Hu et al., 2015). These issues need further investigation.

Generally, there are two commonly used optimization strategies to restrain the numerical dissipation of classical WENO schemes. One strategy has been widely applied by adopting hybrid approaches (Adams and Shariff, 1996; Pirozzoli, 2002). However, the complexity of coupling two separate schemes and the transition between the sub-schemes may incur numerical instabilities, particularly when multiple discontinuities are closely located (Larsson and Gustafsson, 2008). Another solution is to modify the weighting strategy for the flux reconstruction process of WENO schemes. This strategy is easily applied and is more suitable for multi-dimensional simulation than the former one. Recently, methods to increase the possible higher-order accuracy in smooth regions have been widely investigated. WENO-M (Henrick et al., 2005) scheme was firstly proposed by employing a mapping function to fix the problem of order degeneration of WENO-JS (Jiang and Shu, 1996) near critical points. A similar method was also employed in WENO-Z (Borges et al., 2008), WENO-RL, and WENO-RLTV (Taylor et al., 2007) schemes to modify weighting formulas. Another method adopted in WENO-SYMOO and WENO-SYMBO (Martín et al., 2006) schemes was adding the effect of the downwind substencil, and employing the optimal weights for the central stencil, rather than for the upwind stencil.

In particular, Hu et al. (2010) developed a central-upwind WENOCU6 scheme which can achieve sixth-order accuracy in smooth regions by introducing an optimal central substencil and a new constant parameter C to increase the contribution of optimal weights. Hu et al. (2010) further pointed out that the magnitude of the parameter C can significantly change the numerical dissipation and stabilities in problems involving strong shock waves. Adopting large values of the parameter C, the schemes can achieve small numerical dissipation in smooth regions. However, doing that also induces obvious numerical instability in the vicinity of discontinuities. On the other hand, with small values of the parameter C, the schemes can preserve stable shock-capturing ability but with obvious dissipation in smooth regions. It is not easy to balance low dissipation and stability when using a single constant C. Therefore, Hu et al. (2010) adopted a moderate constant value C=20 for WENOCU6. Instead of following Hu et al. (2010), Zhao et al. (2019a) proposed a smart method to dynamically adjust the parameter C by employing a binary form switch according to the variation of the local flow-field property. That was to apply $C_{\min}$ ($C_{\min}$=C=20) near shocks while using $C_{\max}$ (reference value $C_{\max}$=200) in smooth regions to improve the performance of schemes, especially for restraining the numerical dissipation in smooth regions. This method overcame the insufficiency of the usage of a constant small value, and the optimized scheme showed some improvement compared with the baseline scheme.

The forth-order WENOCU4, as one of the typical WENOCU schemes, is inferior to WENOCU6 in accuracy, but it is more suitable for engineering applications due to its moderate cost-efficient properties compared to other same-order shock-capturing schemes. Generally, it is not easy to balance high-order accuracy and strong robustness. The higher-order schemes are likely to incur numerical instabilities (Fleischmann et al., 2019). That is to say, C=20 as well as $C_{\max}$=200 may be not suitable for WENOCU4. Theoretically, WENOCU4 could adopt larger values due to its lower-order accuracy. Such reference values for the WENOCU4 scheme are not found in the literature and thus the issue deserves further research. Another point that should be noted is that an efficient parameter C switch plays a critical role for the accurate and stable transition between $C_{\max}$ and $C_{\min}$. However, only a binary switch with a Boolean operation has been employed for the construction of the adaptive parameter C (Zhao et al., 2019a). The performance of other continuous form switches needs further analysis and evaluation. As we know, the same switch form as that of Zhao et al. (2019a), but without a Boolean operation, can be regarded as a simple continuous switch. Wu and Zhao (2015) also developed a hyperbolic tangent switch that shows good performance.

This current work extends that previous research. We provide the reference values of the parameter C (generally, $C_{\min}$=C) and $C_{\max}$ for the optimized WENOCU4 scheme. Meanwhile, the comprehensive performance of the aforementioned

three switches is evaluated and analyzed, including dispersion and dissipation properties and computational efficiency. We emphasize that although the analysis of switches is only carried out for a particular scheme, namely WENOCU4, we shall be using the optimized WENOCU4 scheme for engineering applications in further studies. The evaluations for switches have general validity, hence they can, in principle, be extended for the improvement of other WENO schemes, especially the ones based on WENOCU schemes.

The outline of the paper is as follows: First, we present the introduction and function of the parameter C and the rationale of three different kinds of switches. Then, the reference values of the adaptive parameters C are investigated and the comprehensive properties of switches are evaluated by a wide range of benchmark test cases, including 1D scalar problems, empirical dispersion relation (EDR) analysis in the wavenumber space, and applicative examples to the multi-dimensional Euler equations.

2 Numerical methods

2.1 Central-upwind fourth-order WENOCU4 scheme

Assuming that the flowing fluid is compressible without viscidity, we briefly present the development of the WENO scheme for the 1D advection equation in the scalar form.

$$\frac{\partial u}{\partial t}+\frac{\partial f(u)}{\partial x}=0,\ u(x,0)=u_0(x),\quad -\infty<x<+\infty, \tag{1}$$

where t is the non-dimensional time, u denotes the conservative variable, u_0 is the variable at initial time, and $f(u)$ is the associated numerical flux. Assuming a uniform mesh with grid points x_i, a finite-difference semi-discretized version of Eq. (1) is as follows:

$$\frac{\mathrm{d}v_i}{\mathrm{d}t}=-\frac{1}{h}\left(\hat{f}_{i+1/2}-\hat{f}_{i-1/2}\right)\approx\left.\frac{\partial f(u)}{\partial x}\right|_i, \tag{2}$$

where $v_i(t)\approx u(x_i, t)$, and $\hat{f}$ is the numerical flux at the cell interface $x_{i+1/2}$ with uniform spacing h. The classical $(2r-1)$-order WENO scheme adopts a $(2r-1)$-point global stencil, which is subdivided into r substencils $\{S_0, S_1, \ldots, S_{r-1}\}$ with each substencil containing r grid points. The numerical approximations of $\hat{f}_{i+1/2}$ are constructed by a convex combination of $\hat{f}_{k,i+1/2}$. For simplicity, here we describe only the interpolation of variables at the left cell boundary $x_{i+1/2}$.

$$\hat{f}_{i+1/2}=\sum_{k=0}^{r-1}\omega_k\hat{f}_{k,i+1/2}. \tag{3}$$

As for the classical WENO3 scheme, the two-point substencils S_0 and S_1 are used to reconstruct the flux at $x_{i+1/2}$ and the nonlinear weights ω_k as follows:

$$\omega_k=\frac{\alpha_k}{\sum_{k=0}^{1}\alpha_k},\ \alpha_k=\frac{d_k}{(\varepsilon'+\beta_k)^2},\quad k=0,1, \tag{4}$$

where α_k denotes the un-normalized weight, d_k denotes the optimal weight, β_k denotes the smoothness indicator, and the parameter ε' is to avoid division by zero in the denominator.

Borges et al. (2008) further proposed a general framework for the WENOZ scheme. A whole three-point substencil S_3 was introduced to devise a new smoothness indicator τ_3:

$$\tau_3=\left|\beta_0-\beta_1\right|. \tag{5}$$

However, there are still only the two-point upwind substencils (S_0 and S_1) that are used, and the nonlinear weights ω_k are defined by

$$\omega_k=\frac{\alpha_k}{\sum_{k=0}^{1}\alpha_k},\ \alpha_k=d_k\left(1+\frac{\tau_3}{\varepsilon'+\beta_k}\right),\quad k=0,1. \tag{6}$$

Inspired by the aforementioned idea, Hu et al. (2010) proposed a general framework for the WENOCU scheme. The classical WENOCU4 scheme is derived based on WENO3Z by introducing an optimal central substencil. Fig. 1 shows the flux reconstruction process for the left-biased WENO3, WENO3Z, and WENOCU4 at $x_{i+1/2}$.

Specifically, WENOCU4 introduces the contribution from the downwind substencil S_2 to

reconstruct the central substencil with the highest order of accuracy for optimal weights. The nonlinear weights ω_k are given by Eq. (7). While Eq. (7) has a similar form to Eq. (6), the smoothness indicator β_2 for the downwind substencil is replaced by β_4 for the optimal four-point central substencil. Besides, a new constant parameter $C\gg1$ is introduced to increase the contribution of optimal weights when the smoothness indicators have comparable magnitudes (Taylor et al., 2007).

$$\omega_k=\frac{\alpha_k}{\sum_{k=0}^{2}\alpha_k},\ \alpha_k=d_k\left(C+\frac{\tau_4}{\beta_k+\varepsilon'}\right),\quad k=0,1,2, \tag{7}$$

where τ_4 is the new reference smoothness indicator. The optimal weights d_k are given by

$$d_0=\frac{1}{6},\ d_1=\frac{2}{3},\ d_2=\frac{1}{6}. \tag{8}$$

The functions of smoothness indicators β_k are defined as

$$\begin{cases}\beta_0=\left(-f_{i-1}+f_i\right)^2,\\ \beta_1=\left(-f_i+f_{i+1}\right)^2,\\ \beta_2=\left(-f_{i+1}+f_{i+2}\right)^2,\\ \beta_4=\dfrac{1}{36}\left(-2f_{i-1}-3f_i+6f_{i+1}-f_{i+2}\right)^2\\ \quad+\dfrac{13}{12}\left(f_{i-1}-2f_i+f_{i+1}\right)^2\\ \quad+\dfrac{781}{720}\left(-f_{i-1}+3f_i-3f_{i+1}+f_{i+2}\right)^2.\end{cases} \tag{9}$$

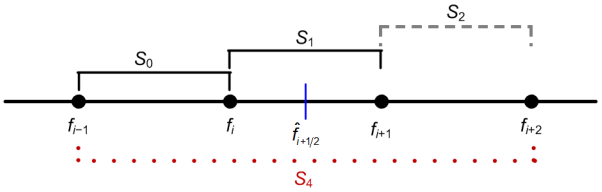

Fig. 1 Stencils for left-biased WENO3, WENO3Z (solid lines), and WENOCU4 (dotted and dashed lines) flux reconstruction at $x_{i+1/2}$

Using a Taylor expansion to β_k gives

$$\begin{cases}\beta_0=f'^2\Delta x^2+\dfrac{1}{4}f''^2\Delta x^4-ff''\Delta x^3\\ \quad+\dfrac{1}{3}ff'''\Delta x^4+O\left(\Delta x^5\right),\\ \beta_1=f'^2\Delta x^2+\dfrac{1}{4}f''^2\Delta x^4+ff''\Delta x^3\\ \quad+\dfrac{1}{3}ff'''\Delta x^4+O\left(\Delta x^5\right),\\ \beta_2=f'^2\Delta x^2+\dfrac{9}{4}f''^2\Delta x^4+3ff''\Delta x^3\\ \quad+\dfrac{7}{3}ff'''\Delta x^4+O\left(\Delta x^5\right),\\ \beta_4=f'^2\Delta x^2+\dfrac{13}{12}f''^2\Delta x^4+O\left(\Delta x^5\right),\end{cases} \tag{10}$$

where $O(\cdot)$ denotes the Taylor remainder.

$\hat{f}_{k,i+1/2}$ means the substencil fluxes obtained from the node value f_i as

$$\begin{cases}\hat{f}_{0,i+1/2}=-\dfrac{1}{2}f_{i-1}+\dfrac{3}{2}f_i,\\ \hat{f}_{1,i+1/2}=\dfrac{1}{2}f_i+\dfrac{1}{2}f_{i+1},\\ \hat{f}_{2,i+1/2}=\dfrac{3}{2}f_{i+1}-\dfrac{1}{2}f_{i+2},\\ \hat{f}_{4,i+1/2}=-\dfrac{1}{12}f_{i-1}+\dfrac{7}{12}f_i+\dfrac{7}{12}f_{i+1}-\dfrac{1}{12}f_{i+2}.\end{cases} \tag{11}$$

The new reference smoothness indicator τ_4 can be obtained by

$$\begin{aligned}\tau_4&=\beta_4-\left(\frac{\beta_0+\beta_1}{2}\right)\\ &=\frac{5}{6}f''^2\Delta x^4-\frac{1}{3}ff'''\Delta x^4+O\left(\Delta x^5\right)=O\left(\Delta x^4\right).\end{aligned} \tag{12}$$

With large values of the parameter C, the numerical dissipation in smooth regions can be restrained. Unfortunately, it also brings spurious numerical oscillations near discontinuity regions. On the other hand, with small values of the parameter C, the shocks can be stably captured. However, that brings obvious dissipation in smooth regions. Hu et al. (2010) thought the constant parameter C should be of order $O(10)$ for WENOCU6 scheme. Therefore, they

employed a constant C=20 for WENOCU6. However, the usage of a constant low value is insufficient and the applicability of directly employing C=20 for WENOCU4 needs further analysis.

2.2 Three adaptive switches for dynamically adjusting parameter C

The adaptive parameter C requires provisional detection of the smoothness of regions to achieve accurate and stable algorithms. A novel efficient shock sensor proposed by the present authors with a weak dependence on user-defined parameters is employed to distinguish the smooth regions and discontinuities. As we know, the rationale of the classical WENO scheme is that the nonlinear weight ω_k associated with a given substencil will be approximately zero near a sharp discontinuity while it will automatically reduce to the corresponding ideal one d_k in the case of a perfectly smooth solution (Jiang and Shu, 1996). Therefore, we devised the sensor θ based on the regularity of the relative deviation between the nonlinear weight ω_k and its corresponding ideal weight d_k. The formula is defined as

$$\theta=\frac{\sum_{k=0}^{\zeta-1}\left|\frac{\omega_k}{d_k}-1\right|^n}{\left|\frac{1}{\min_m d_m}-1\right|^n+(\zeta-1)},\quad m=0,1,\cdots,\zeta-1, \tag{13}$$

where ζ stands for the number of substencils of WENO scheme, n is an exponential parameter controlling the sensitivity to the deviations of nonlinear weights from the ideal ones, k and m both represent the serial number of the substencil. It has been previously proved that no significant effect results from the change of the parameter n (Zhao et al., 2020). For the sake of simplicity and to maintain a moderate sensitivity, we apply n=2. The numerator means the summational relative deviations of weights for a global stencil. The maximum a nonlinear weight can ever attain is ω_k=1. The denominator denotes the maximum value that the numerator can ever attain, that is the substencil where the minimum value of the optimal weight d_m and nonlinear weight ω_k=1 occur simultaneously. It means for normalization purposes, namely $0\le\theta\le1$. This sensor will approach 1 in the vicinity of discontinuities while being zero in smooth regions. The value of this shock sensor is computed by the density variable which has been certified as a suitable property to detect discontinuity (Pirozzoli, 2011).

The efficient parameter C switch acts as a critical role for the accurate and robust transition between $C_{\max}$ and $C_{\min}$. The three different switches evaluated in this study are as follows:

(I) The binary switch (Zhao et al., 2019a) is developed based on the significant difference between the sharp discontinuity and the smooth regions. If the value of shock sensor is greater than a specified threshold value, the position is regarded as a discontinuity and the switch employs $C_{\min}$ to maintain stability. As for other regions, it employs the moderate $C_{\max}$ to restrain numerical dissipation. Therefore, this switch exhibits a straightforward feature, which is defined in Eq. (14), and the WENOCU4 scheme with it is labeled as EWENOCU4_CUT.

$$C=(1-\psi)\times(C_{\max}-C_{\min})+C_{\min}, \tag{14}$$

where $C_{\min}$=C, and $C_{\max}$ is a suitable value to restrain numerical dissipation and preserve stability. The switch works together with a Boolean operation ψ, which is given by

$$\psi=\begin{cases}1, & \text{if } \theta>\xi,\\ 0, & \text{otherwise,}\end{cases} \tag{15}$$

where ξ=0.7 is a reasonable value which has been analyzed in our previous study (Zhao et al., 2020).

(II) The continuous switch directly adopts the value of the shock sensor without introducing a Boolean operation. Therefore, this switch shows a linear transition as the variation of the shock sensor value. This switch is defined as

$$C=(1-\theta)\times(C_{\max}-C_{\min})+C_{\min}, \tag{16}$$

and the WENOCU4 scheme with it is labeled as EWENOCU4_CONT.

(III) The hyperbolic tangent switch (Wu and Zhao, 2015) exhibits a quick variation in the "transition" zone while keeping a slow variation near the "margin" zones when closely approaching sharp discontinuities or perfectly smooth regions. This can

be regarded as a "gentle" manner. However, this complex form shows poor computational efficiency. This switch is defined as shown in Eq. (17), and the WENOCU4 scheme with it is referred to as EWENOCU4_TANH.

$$C=-\left[\frac{1}{2}\frac{\tanh\left(r_{\mathrm{c}}\dfrac{\theta-r_{\mathrm{d}}}{\max\left(\theta,\left|\theta-r_{\mathrm{d}}\right|\right)}\right)}{\tanh r_{\mathrm{c}}}-\frac{1}{2}\right]\times\left(C_{\max}-C_{\min}\right)+C_{\min},\tag{17}$$

where r_{d} and r_{c} denote the parameters controlling the performance of switch. The connection of parameters r_{d} and r_{c} is plotted in Fig. 2. This switch shows several interesting features:

(1) The parameter C varies from $C_{\min}$ to $C_{\max}$ if $r_{\mathrm{d}}\leq 0.5$. Inversely, the value of C cannot attain $C_{\min}$ if $r_{\mathrm{d}}>0.5$.

(2) The parameter r_{d} directly controls the range of the "transition" zone and $C=(C_{\max}+C_{\min})/2$ when $\theta=r_{\mathrm{d}}=0.5$. r_{c} controls the variation gradient of parameter C for a specific r_{d}. The performance of this switch is mainly controlled by r_{d}.

(3) For a smaller value of r_{d}, with increasing θ, the parameter C decreases rapidly around $\theta=0$. Inversely, for a larger r_{d}, with increasing θ, the parameter C decreases slowly around $\theta=0$.

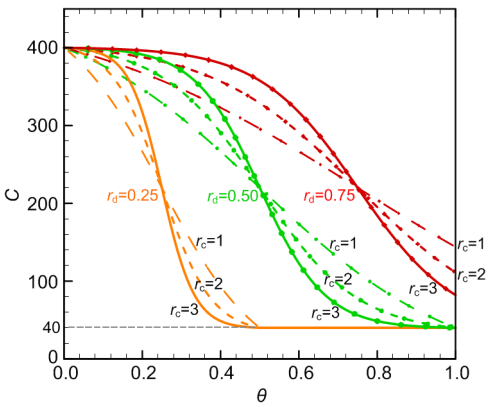

Fig. 2 Relations between parameters C and θ with varying r_{d} and r_{c}

Although adopting critical $r_{\mathrm{d}}=0.5$ is enough in ideal conditions, the stability and robustness of the switch for this case are worthy of further validation. Generally, $r_{\mathrm{d}}=0.25$ and $r_{\mathrm{c}}=3$ are reasonable values and are used in this study. The adaptive parameter C changes to $C_{\min}$ when $\theta\geq 0.5$ and keeps a continuous smooth transition from $C_{\max}$ to $C_{\min}$ elsewhere.

3 Numerical tests and discussion

3.1 Assessments of EWENOCU4 scheme with different switches for scalar equations

In the following subsections, what we contrive to do is to evaluate the comprehensive performance of three different switches by analyzing the dispersion and dissipation properties as well as the computational efficiency of the optimized EWENOCU4 scheme. It needs to be emphasized that excellent shock-capturing schemes should preserve numerical stability near the discontinuity without excessive dissipation contained in smooth regions. Additionally, the schemes should achieve relatively high computational efficiency. We emphasize that, although only a limited number of results are shown in the following sections, all the results are representative.

3.1.1 Shock-capturing error

The sound wave refraction test case is a scalar model which was originally introduced by Casper and Carpenter (1998) and further developed by Zhao et al. (2019b). This test case is employed for modeling the refraction of sound waves at the interface of solid media with different acoustic impedances. This trait is common to almost any aeroacoustic problems that involve shock waves. The shock-capturing capacity, stability, and dissipation properties of schemes can be analyzed. It assumes the linear propagation of sinusoidal disturbances in a medium while the sound speed c changes abruptly. Specifically, Eq. (18) is considered with different sound speed values of $c_1>c_2>0$:

$$c=\begin{cases}c_1, & x\leq 0,\\ c_2, & x>0.\end{cases}\tag{18}$$

The characteristic lines enter the discontinuity standing at $x=0$ from the left and exit from the right, thus making this example a convenient simplified test case to analyze shock-sound interaction problems. Considering incoming sinusoidal disturbances of

amplitude $\varepsilon_1=\varepsilon$ and wavenumber upstream of the discontinuity w_1, the following exact solution is found after an initial transient:

$$u(x,t)=\begin{cases}u_1(x,t)=c_2+\varepsilon_1 \mathrm{e}^{\mathrm{i}w_1(x-c_1t)}, & x\le 0,\\ u_2(x,t)=c_1+\varepsilon_2 \mathrm{e}^{\mathrm{i}w_2(x-c_2t)}, & x>0,\end{cases} \tag{19}$$

where $\varepsilon_2=\varepsilon c_1/c_2$. $w_2=w_1c_1/c_2$ means the spatial wavenumber downstream of the discontinuity and satisfies the Rankine-Hugoniot jump relations:

$$c_1u_1(0,t)=c_2u_2(0,t). \tag{20}$$

For a 1D mesh with uniform spacing h, the reduced wavenumber $\varphi_2=w_2h$ means the spatial wavenumber downstream of the discontinuity per spacing h distance. The solutions are computed on the domain $x\in[-2, 10]$, with the following baseline conditions: $w_1=2\pi$, $\varepsilon=0.1$, $c_1=2$, and $c_2=1$. The "exact" reference result is obtained by WENO5 scheme on a uniform 10001-point mesh.

Fig. 3 presents the results of the WENOCU4 scheme with the reduced wavenumber $\varphi_2=w_2h\approx0.8$, corresponding to 97 points. The WENOCU4 scheme with a constant value $C=1$ (labeled here as WENOCU4_C=1) exhibits excessive dissipation downstream of the discontinuity, while WENOCU4_C=100 shows obvious oscillations upstream of the shock. This illustrates the significant effect of the parameter C. With a number of numerical tests, we find that the moderate value $C=40$ can preserve shock-capturing ability without spurious oscillations or excessive numerical dissipation. The same conclusion can be drawn from the results of Euler equations. If not mentioned otherwise, we set $C=C_{\min}=40$.

We further investigate the effect of the parameter $C_{\max}$ on the solutions with $\varphi_2\approx0.8$. For illustrative purposes, only the typical results with $C_{\max}$=50, 400, 1000, and 10000 of EWENOCU4_CUT are depicted in Fig. 4 although we conducted many investigations. As illustrated, the attenuation associated with the propagation error decays more slowly with increasing $C_{\max}$. $C_{\max}$=50 is too small to exhibit the superiority of the adaptive parameter C while larger $C_{\max}$ can efficiently restrain the numerical dissipation. The reason is that the efficient shock sensor is capable of precisely identifying the shock positions and $C_{\min}$ is only employed near critical cells to maintain numerical stability while $C_{\max}$ is employed elsewhere. This fact will be further illustrated in the following part. Although employing sufficiently large values $C_{\max}$=1000 or 10000 for EWENOCU4 can achieve stable solutions for this case, noticeable oscillations will occur in several problems of Euler equations. Generally, $C_{\max}$=400 is a suitable value that can restrain numerical dissipation to the utmost extent without oscillations. Therefore, unless specified, the EWENOCU4 scheme adopts constant $C_{\max}$=400.

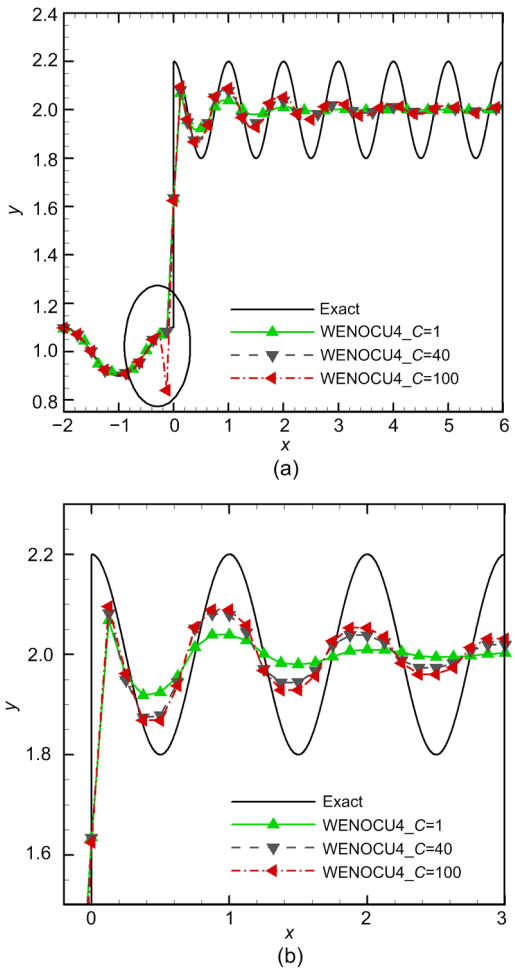

Fig. 3 Computed solutions of the WENOCU4 scheme with increasing value of C for model sound wave refraction test case

(a) Global view; (b) Local view. $\varphi_2=w_2h\approx0.8$ and t=8

Fig. 5 presents the results of various shock-capturing schemes. The reduced wavenumber is set as $\varphi_2\approx0.8$ and we employ $C_{\max}$=400 for the EWENOCU4 scheme. WENOCU4 exhibits the most

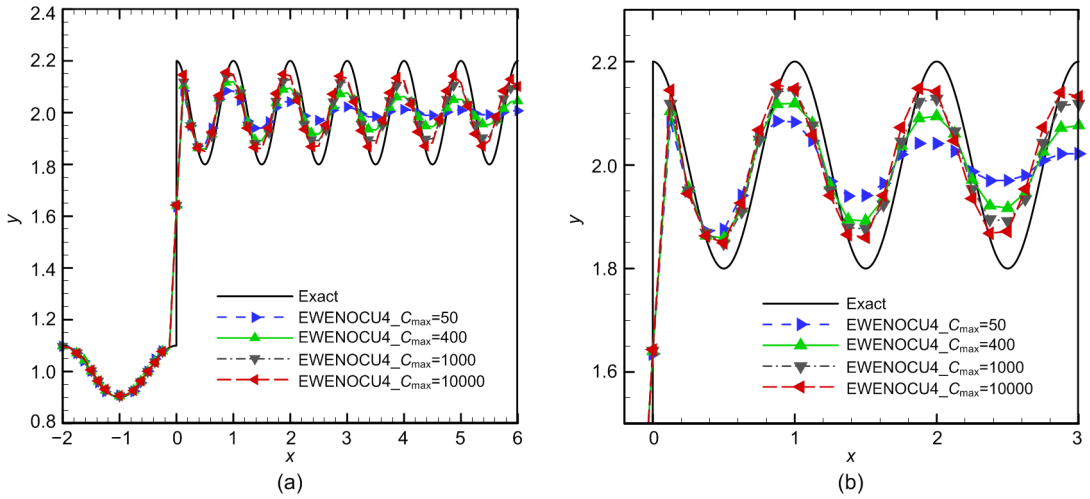

Fig. 4 Computed solutions of EWENOCU4_CUT scheme with increasing value of C_{max} for model sound wave refraction test case

(a) Global view; (b) Local view. $\varphi_2=w_2h\approx0.8$ and $t=8$

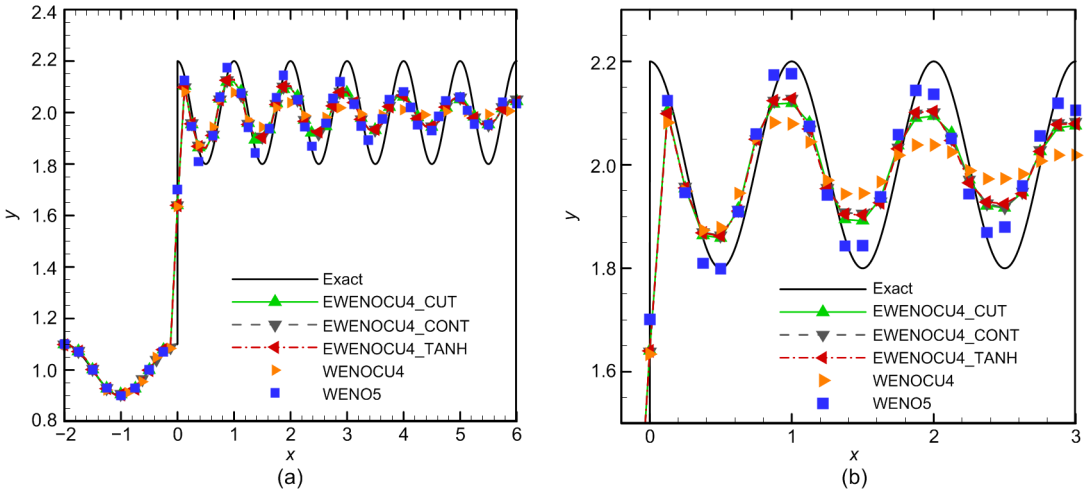

Fig. 5 Computed solutions of various shock-capturing schemes for model sound wave refraction test case

(a) Global view; (b) Local view. $\varphi_2=w_2h\approx0.8$ and $t=8$

dissipation in the post-shock smooth region. EWENOCU4 can achieve notable improvement compared with WENOCU4. However, EWENOCU4 decays faster in smooth regions downstream of the shock compared to WENO5, which may be due to the limited two-point length of upwind substencils within the reconstruction process of the baseline WENOCU4 scheme. Moreover, EWENOCU4 with any types of switches shows similar performance.

Fig. 6 compares the solutions of EWENOCU4 with different switches. These results can explain why EWENOCU4 tends to achieve better results than the baseline WENOCU4 scheme. As can be seen, the locations of strong shock are perceived precisely by the efficient shock sensor and C_{min} is triggered near critical cells at barely three points while a larger parameter C is employed elsewhere. As for the region near the shock, the parameter C profile of the binary switch shows a sharp transition while the other two both exhibit a gradual transition. Certainly, all the solutions are stable without oscillations. It can be appreciated that once the discontinuities are accurately identified and employ corresponding C_{min} to guarantee their stability, a binary transition or not

near the shock region has little effect on the numerical stability. However, different switches give obvious discrepancies in the smooth regions, that is all the smooth zones employ $C_{\max}$ for the binary switch while the other switches will not attain $C_{\max}$ at several points (defined here as misidentification). Therefore, the binary switch can efficiently filter the misidentifications in smooth regions. This is mainly due to the function of the threshold within the Boolean operation, while the other switches directly compute the values of the shock sensor. Therefore, EWENOCU4_CONT and EWENOCU4_TANH are more dissipative compared to EWENOCU4_CUT from a theoretical standpoint, although the discrepancy is not significant. The results indicate the high resolution of the shock sensor and the superiority of the EWENOCU4 scheme for capturing shocks with necessary dissipation and for resolving smooth flow features with low dissipation properties. Generally, the robustness and low-dissipation property of EWENOCU4_CUT are satisfactory.

3.1.2 Empirical dispersion relation

Here, we investigate the spectral property of the EWENOCU4 scheme with different switches by using EDRs (Pirozzoli, 2006). The EDR method is capable of quantifying the leading order for nonlinear effects of discretization schemes in whole wavenumbers. We consider the 1D propagation of small disturbances in a periodic domain, governed by the linear advection equation, with monochromatic sinusoidal initial conditions of wavelength λ and the corresponding wavenumber $w=2\pi/\lambda$.

$$\frac{\partial u}{\partial t}+a\frac{\partial u}{\partial x}=0,\quad u(x,0)=\hat{u}_0\mathrm{e}^{\mathrm{i}wx}, \tag{21}$$

where a is the advection speed, and $\hat{u}_0$ is the complex amplitude of the mode of the solution at the initial condition. A semi-discrete approximation of Eq. (21) on a uniform mesh with spacing h and nodes $x_j=jh$ is given by

$$\frac{\mathrm{d}v_j}{\mathrm{d}t}+a\mathrm{D}v_j=0,\quad v_j(0)=\hat{u}_0\mathrm{e}^{\mathrm{i}j\varphi}, \tag{22}$$

where $v_j(t)\approx u(x_j,\ t)$, $\varphi=wh$ denotes the ideal wavenumber, and D means a general (linear or nonlinear) space derivative approximation. In the case of linear approximations, that is

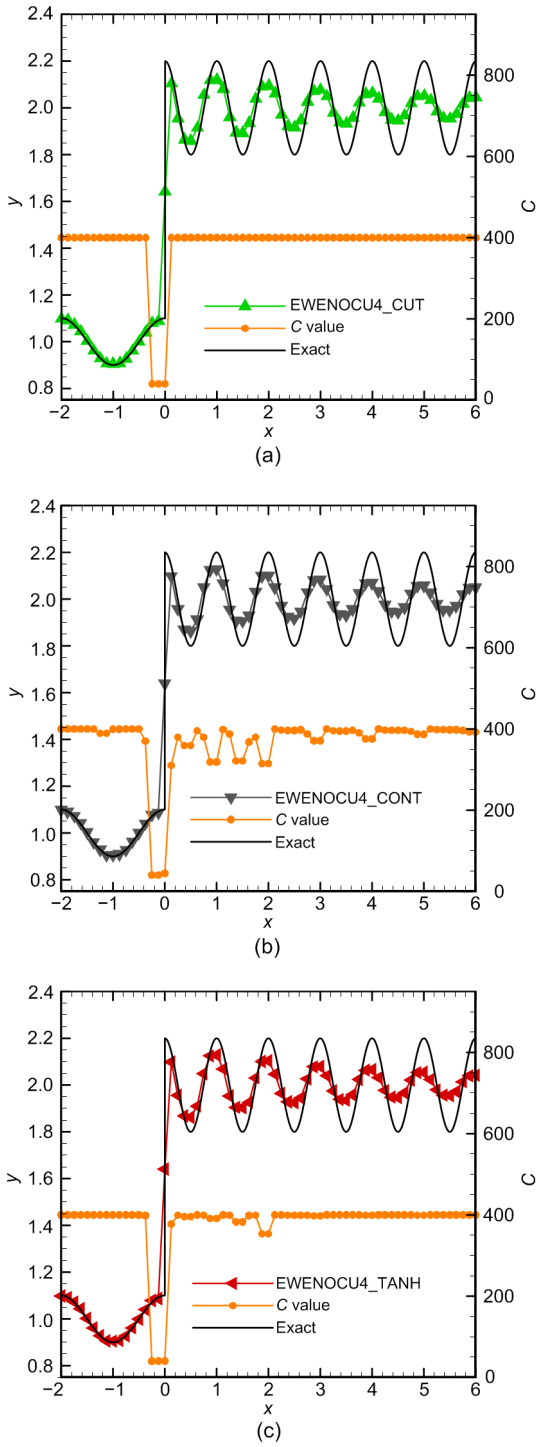

Fig. 6 Computed solutions of EWENOCU4 scheme with different switches for model sound wave refraction test case

(a) EWENOCU4_CUT; (b) EWENOCU4_CONT; (c) EWENOCU4_TANH. $\varphi_2=w_2h\approx0.8$ and $t=8$

$$\mathrm{D}v_j = \frac{1}{h}\sum_{l=-q_1}^{q_2} a_l v_{j+l} \approx \left.\frac{\partial u}{\partial x}\right|_{x=x_j}, \tag{23}$$

where q_1 and q_2 denote the lower and upper bounds, respectively, and a_l denotes the weight coefficient. The exact solution of Eq. (22) is as follows:

$$v_j(t) = \hat{v}(t)\mathrm{e}^{\mathrm{i}j\varphi}, \tag{24}$$

where the complex amplitude of the solution at time t is given by

$$\hat{v}(t) = \mathrm{e}^{-\mathrm{i}\left(\frac{at}{h}\right)\Phi(\varphi)}\hat{u}_0, \tag{25}$$

where $\Phi(\varphi)$ is the modified wavenumber (Lele, 1992) associated with the ideal wavenumber, and the space discretization is defined by

$$\Phi(\varphi) = \frac{1}{\mathrm{i}}\sum_{l=-q_1}^{q_2} a_l \mathrm{e}^{\mathrm{i}l\varphi}. \tag{26}$$

Ideally, $\Phi(\varphi)=\varphi$. However, that cannot be always realized. Therefore, the relative deviation between the modified wavenumber and its corresponding ideal wavenumber can be used to analyze the relative error of schemes.

For nonlinear approximations of the space derivative operator, we can introduce the EDR by advancing the solution up to a very short time τ', in order to rule out any error associated with time integration. The Fourier transform of the solutions at time τ' yields the complex amplitude of the mode associated with the reduced wavenumber φ, labeled as $\hat{v}(\varphi;\tau')$. The modified wavenumber $\Phi(\varphi)$ can be derived from Eq. (26) as follows:

$$\Phi(\varphi) = -\frac{1}{\mathrm{i}\sigma}\ln\frac{\hat{v}(\varphi;\tau')}{\hat{u}_0(\varphi)}, \tag{27}$$

where $\sigma=a\tau'/h=1$. Repeating the aforementioned procedures we can obtain the results in the whole wavenumber space. The deviation of the real part of modified wavenumber Φ from the ideal wavenumber φ ($\mathrm{Re}\Phi(\varphi)$) is associated with the dispersion property, while the imaginary part of Φ ($\mathrm{Im}\Phi(\varphi)$) is associated with the dissipation property.

Fig. 7 shows the solutions of EDR. Firstly, we focus on the effect of the magnitude of the parameter C on the behavior of WENOCU4. As can be seen, the larger value of C corresponds to less numerical dissipation. The analysis also indicates that WENOCU4_C=1 induces obvious instability at high wavenumbers, where $\mathrm{Re}\Phi(\varphi)<0$. Similar to the results of the model sound wave refraction test case, increasing the parameter $C_{\max}$ has a diminished improvement on the performance of the EWENOCU4 scheme when the value of $C_{\max}$ is about one order of magnitude larger than $C_{\min}$=40. Certainly, the larger $C_{\max}$ corresponds to better numerical performance for this test case.

The EWENOCU4 scheme with different switches exhibits similar results except for a slight difference in high wavenumber regions. Compared with other schemes, the EWENOCU4 scheme can achieve noticeably less numerical dissipation, especially at high wavenumbers. It indicates that employing adaptive switches indeed improves the performance of the scheme. Interestingly, the WENO5 scheme is closer to the ideal spectral properties than WENOCU4-based schemes at low wavenumbers whereas it departs quicker at high wavenumbers. That indicates that, at relatively coarse grids, WENO5 may induce worse solutions compared to other schemes.

The EDR given above can be used to evaluate the computational efficiency of the algorithm. Table 1 displays the estimated central processing unit (CPU) time per grid point per time step cost by the various schemes, normalized by the CPU time required by the WENO5 scheme. Although WENOCU4 requires a similar computational cost to WENO5, it achieves better performance in the wavenumber space. As we expect, EWENOCU4_CUT and EWENOCU4_CONT exhibit similar efficiency, while EWENOCU4_TANH is the least efficient due to the complex form of the hyperbolic tangent switch. The computational cost of the EWENOCU4 scheme is heavier compared to WENOCU4 due to the additional computation of the shock sensor and adaptive switches. However, the greater computational cost is a worthwhile sacrifice for less numerical dissipation and for capturing discontinuities stably (see the solutions of Euler equations in Figs. 8–23).

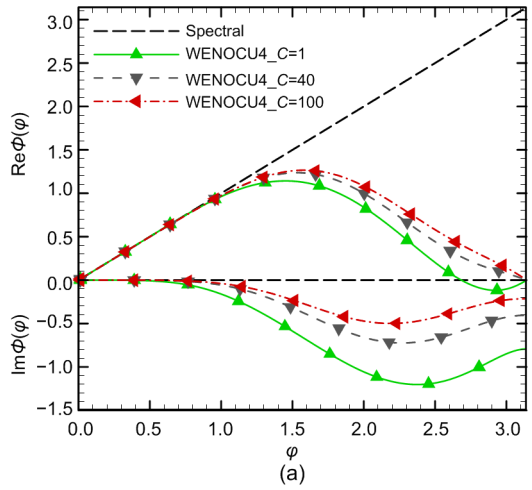

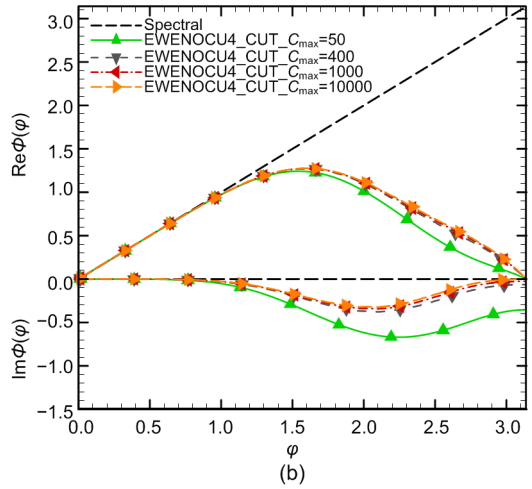

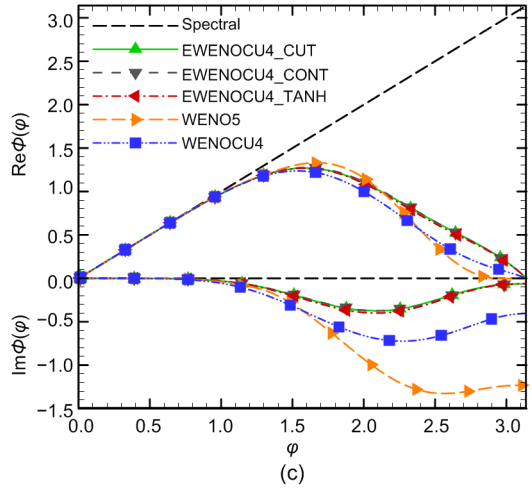

Fig. 7 EDR analyses for several shock-capturing schemes
(a) WENOCU4 with increasing value of C; (b) EWENOCU4 with increasing value of C_{max}; (c) Comparison of several schemes. The deviations of the real and imaginary parts of the modified wavenumber Φ from the ideal φ are associated with numerical dispersion and dissipation properties, respectively

Table 1 Estimated CPU time per grid point per time step for various schemes, normalized by the WENO5 scheme

Scheme	CPU time
WENO5	1.000
WENOCU4	1.011
EWENOCU4_CUT	2.893
EWENOCU4_CONT	2.930
EWENOCU4_TANH	3.462

3.2 Applications to 1D Euler equations

In the following sections, we evaluate the performance of switches through multi-dimensional benchmark cases of Euler equations, which have been widely analyzed in the literature. Note that the Roe average approximation is employed for the characteristic decomposition at the cell faces, the Lax-Friedrichs splitting is applied to the numerical fluxes, and the third-order total variation diminishing (TVD) Runge-Kutta method is utilized for time discretization.

3.2.1 Shock-tube problem

Two classical 1D standard shock-tube problems are considered to investigate the performance of EWENOCU4 schemes for resolving steady shocks, contact discontinuities, and rarefaction waves. Almost all the high-order shock-capturing schemes will encounter slight post-shock oscillations, and no complex smooth structures are involved in these problems, so we focus on the signs of wiggles or oscillations downstream of the shocks.

The first one is the Lax problem (Lax, 1954), with Riemann initial conditions (non-dimensional density ρ, velocity v_x, and pressure p) given as

$$(\rho, v_x, p)=\begin{cases}(0.445, 0.698, 3.528), & -5\le x<0,\\ (0.500, 0.000, 0.571), & 0\le x\le 5.\end{cases} \tag{28}$$

The non-dimensional final time is t=1.3.

The second one, namely, the Sod problem (Sod, 1978) consists of the propagation of a shock wave and a contact discontinuity. The initial conditions are given as

$$(\rho, v_x, p)=\begin{cases}(1.000, 0.000, 1.000), & -5\le x<0,\\ (0.125, 0.000, 0.100), & 0\le x\le 5.\end{cases} \tag{29}$$

The computational final time is t=2.

For these two problems, the solutions are both computed on the domain $x\in[-5, 5]$. For $t\le t_{end}$, waves created by the discontinuity at (x, t)=(0, 0) do not reach the boundaries, where a Dirichlet boundary, that is condition(x_B, t)=condition(x_B) $\forall t$ is applied, where x_B means the locations of the boundaries. Both the "exact" reference solutions are obtained by the WENO5 scheme on a 10001-point grid.

As illustrated in Fig. 8, we examine the effect of the magnitude of the parameter C on 200 cells. WENOCU4_C=1 produces excessive smearing effects in the vicinity of discontinuities. On the other hand, an apparent sign of spurious wiggles can be observed for WENOCU4_C=100. With a variety of numerical tests, it is further demonstrated that C=40 is a suitable value, which is similar to the results in Section 3.1.1.

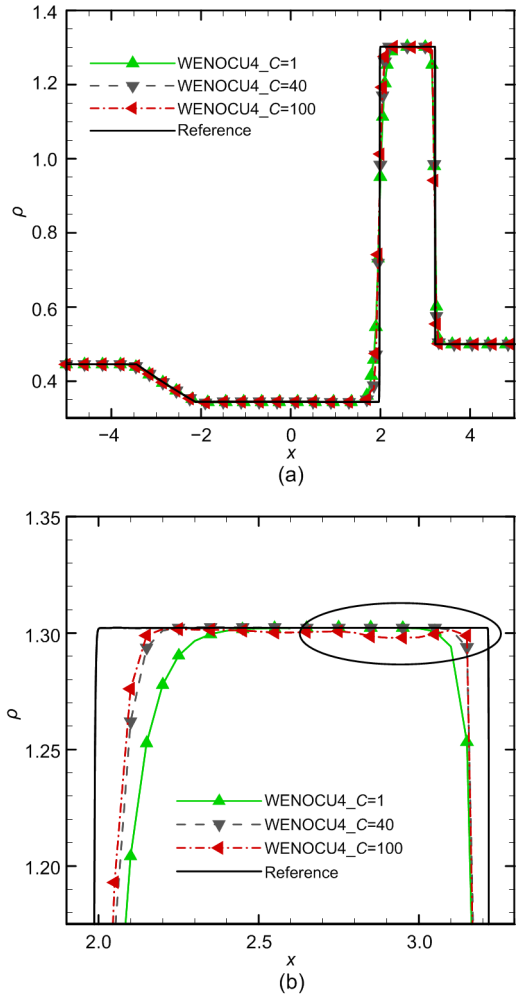

Fig. 8 Density distribution of Lax problem for WENOCU4 scheme with increasing value of C using 200 cells
(a) Global view; (b) Local view

Fig. 9 gives the density profiles of the EWENOCU4_CUT scheme with increasing value of C_{max}. It can be found that with a sufficiently large C_{max} there will be numerical instability. For this problem, slight post-shock oscillations can be observed for the solutions with C_{max}=600, 800, and 1200. Many numerical tests further confirm the rationality of C_{max}=400 without oscillations induced near shocks.

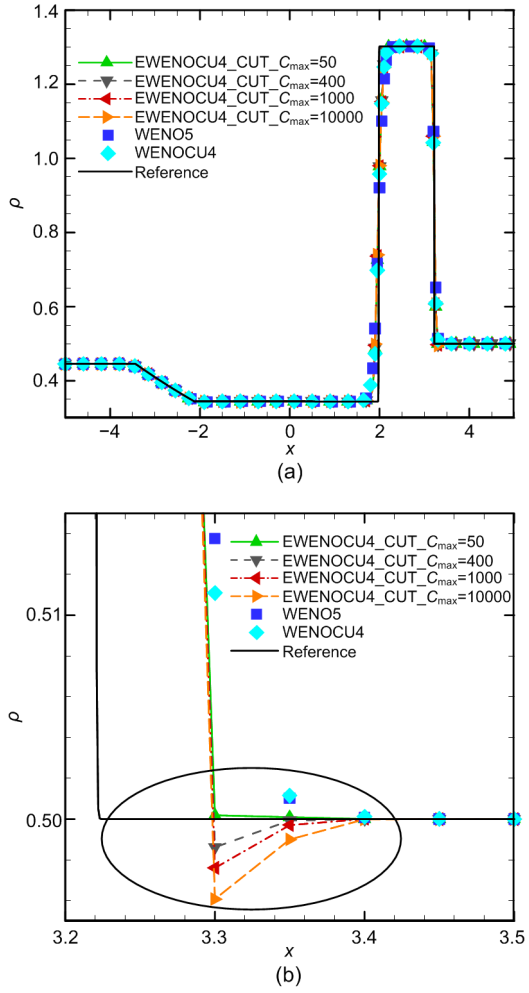

Fig. 9 Density distribution of Lax problem for the EWENOCU4_CUT scheme with increasing value of C_{max} using 200 cells
(a) Global view; (b) Local view

Fig. 10 compares the solutions of different schemes. All schemes are capable of capturing stable

discontinuities. Due to excessive numerical dissipation, the WENO5 scheme achieves the smoothest density distribution around the discontinuity regions, followed by WENOCU4. As can be seen, the EWENOCU4 scheme exhibits a slight sharper density profile. Moreover, no significant difference can be observed for solutions with any type of switches.

To allow for a better comparison of the EWENOCU4 scheme, Fig. 11 displays the parameter C and density distributions. The results show that only sufficient sharp fronts are identified as shocks and smaller C are employed, which explains why EWENOCU4 tends to achieve better results. It is worthwhile to note that the optimized WENOCU4 schemes with different switches exhibit different features. The binary switch, which only applies $C_{\min}$ near discontinuities, shows a straightforward feature while other switches exhibit gradual transitions from $C_{\max}$ to $C_{\min}$. Interestingly, the adaptive parameter C

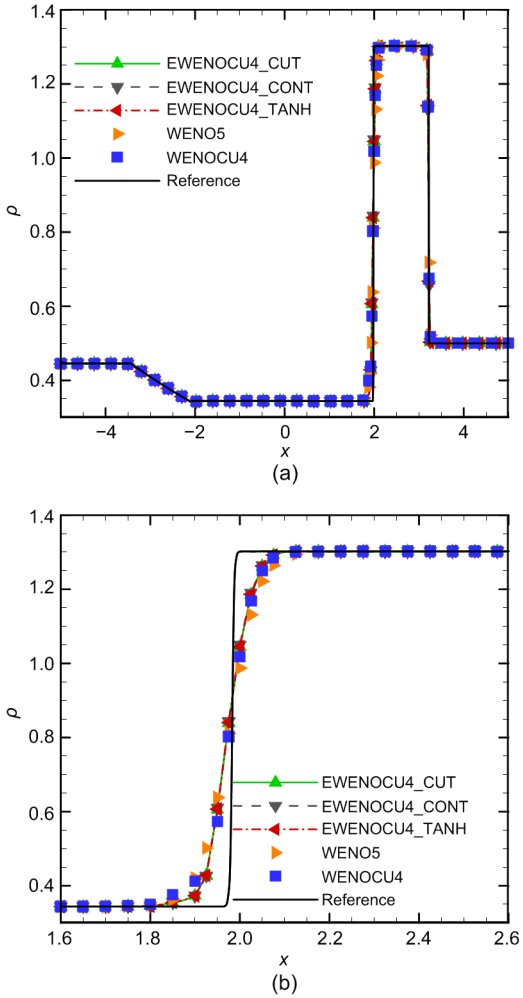

Fig. 10 Density distribution of Lax problem for various shock-capturing schemes using 400 cells
(a) Global view; (b) Local view

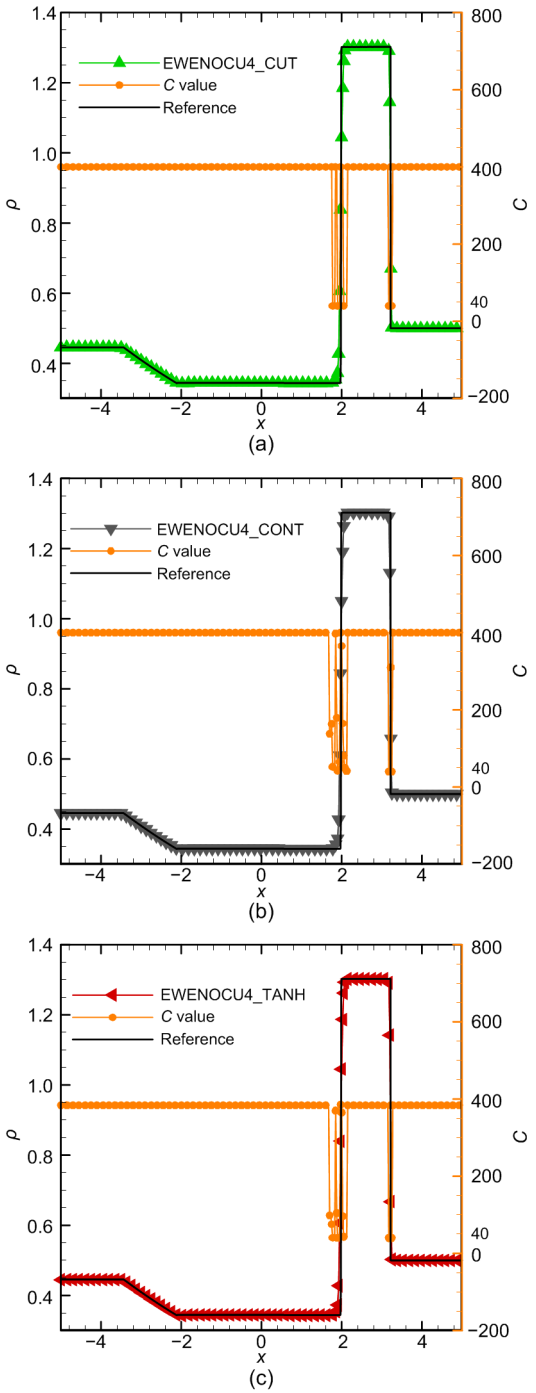

Fig. 11 Density and parameter C distributions of Lax problem for the EWENOCU4 scheme with different switches using 400 cells
(a) EWENOCU4_CUT; (b) EWENOCU4_CONT; (c) EWENOCU4_TANH

may change back to C_{max} near the discontinuity at several points. It is mainly due to the limited-width substencil used by the shock sensor for provisional detection of the smoothness of regions. Generally, no oscillation is incurred and no distinct misidentification is observed for the smooth regions. Similar features can also be observed from other 1D Euler cases.

The effect of the constant C on numerical stability is further revealed in the Sod case. Figs. 12 and 13 depict the solutions of schemes with mesh resolutions of 1/100 and 1/400, respectively. As can be seen, WENOCU4_C=1 produces excessive numerical dissipation and WENOCU4_C=100 shows significant oscillations near the strong shock at x=3.5. A variety of tests further proved that C=40 is a moderate value.

To allow for more detailed comparisons of the numerical solutions with increasing C_{max}, Fig. 13 plots the density distribution and a close-up view downstream of the shock region. As can be seen, all solutions except EWENOCU4_CUT scheme with C_{max}=400 exhibit slight post-shock oscillations, especially for the solution with C_{max}=1200. Moreover, Fig. 14 shows that the EWENOCU4 scheme with C_{max}=400 achieves a slight sharper representation of the shocks compared to WENOCU4 and WENO5. It

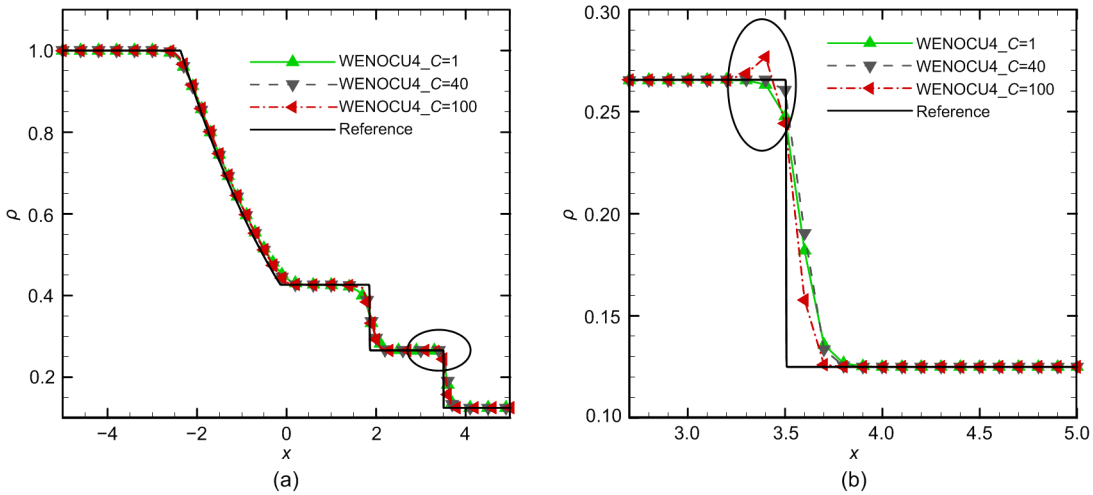

Fig. 12 Density distribution of Sod problem for WENOCU4 scheme with increasing value of C using 100 cells
(a) Global view; (b) Local view

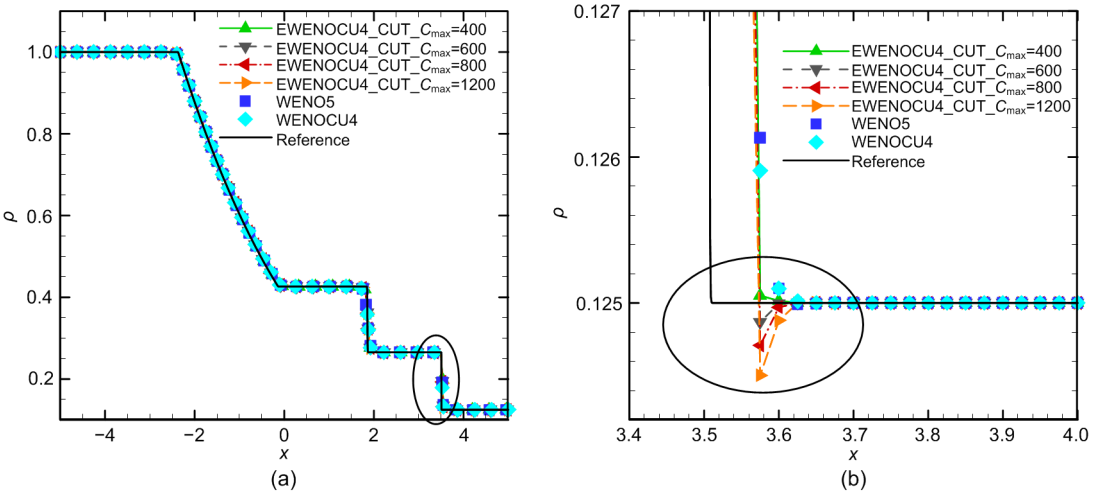

Fig. 13 Density distribution of Sod problem for EWENOCU4_CUT scheme with increasing value of C_{max} using 400 cells
(a) Global view; (b) Local view

indicates the superiority of using the adaptive parameter C and the rationality of C_{max}=400.

Fig. 15 shows the comparison of the EWENOCU4 schemes with different switches. Similarly, EWENOCU4 with the binary switch exhibits a sharp transition near the critical zone while with other switches show a gradual transition between C_{max} and C_{min}.

3.2.2 Shock/entropy wave interaction

The standard 1D Shu-Osher problem is widely preferred because the solution of this test case consists of a main strong shock, multiple shocklets, and a high-gradient smooth post-shock region; all of these are quite challenging ways of testing the simultaneous wave-resolving and shock-capturing abilities of schemes.

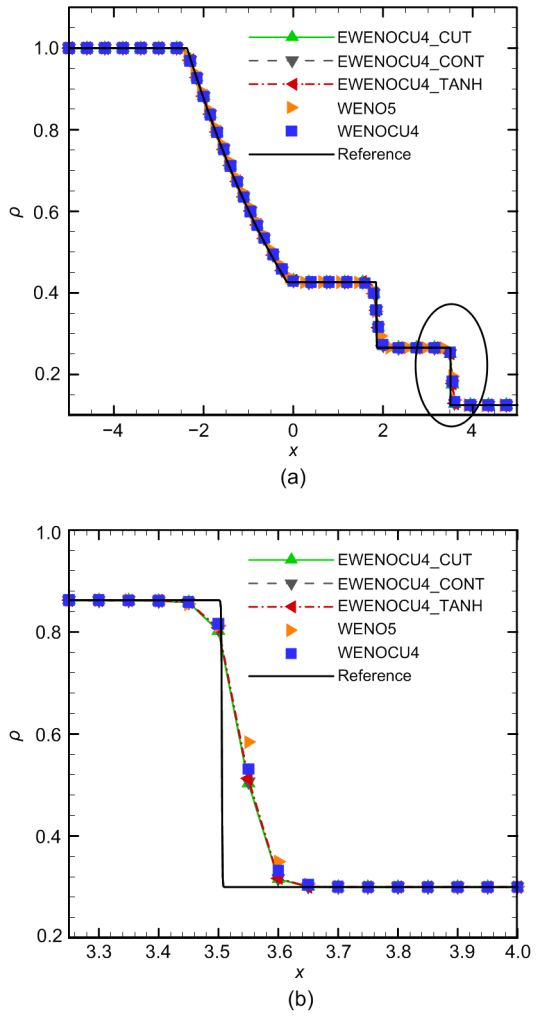

Fig. 14 Density distribution of Sod problem for various shock-capturing schemes using 200 cells
(a) Global view; (b) Local view

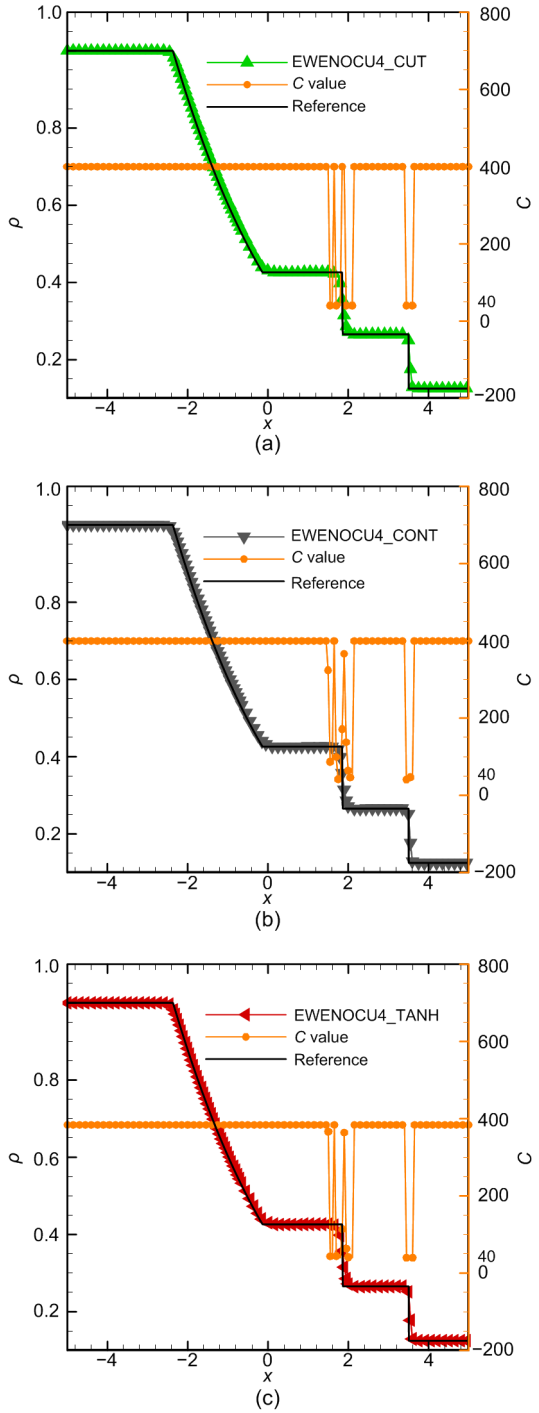

Fig. 15 Density and parameter C distributions of Sod problem for the EWENOCU4 schemes with different switches using 200 cells
(a) EWENOCU4_CUT; (b) EWENOCU4_CONT; (c) EWENOCU4_TANH

An entropy wave interacts with density fluctuations $\Delta\rho$=0.2 across a steady main shock with Mach number Ma=3, with initial conditions as:

$$(\rho, v_x, p)=\begin{cases}(3.85714, 2.629369, 10.33333), & x<-4,\\ (1+0.2\sin(5x), 0, 1), & x\geq -4.\end{cases} \tag{30}$$

The solutions are computed on the domain $x\in[-5, 5]$ and evolved until final time t=1.8. The solution variables remain fixed at the boundaries. The left boundary is supersonic inflow, and at the right boundary, the flow is stagnant, and the pressure is locally uniform during the course of the simulation. Thus, the initial state is maintained at the right boundary. The numerical solutions are computed on a 401-point grid with the result obtained by the WENO5 scheme on a 4001-point grid as a "exact" reference solution.

Fig. 16 shows the computed density and entropy wave profiles. The WENO5 scheme is the least dissipative one while the WENOCU4 scheme is the most dissipative one. The EWENOCU4 scheme with any adaptive switches occupies an intermediary position. It can be noticed that EWENOCU4 achieves a better representation of the amplitudes of density and entropy waves after crossing the multiple shocklets than WENOCU4, whereas it performs worse than WENO5. That is chiefly because the lengths of upwind stencils for EWENOCU4 are less than those of WENO5. Moreover, there are no obvious differences among the results from EWENOCU4 with different switches.

The density and entropy profiles, as well as parameter C distributions obtained by EWENOCU4, are shown in Fig. 17. It can be observed that the main shock and multiple shocklets are detected accurately by the shock sensor. However, several points in the zone of high-frequency entropy waves are misidentified as discontinuities and $C_{\min}$ is employed. That is mainly incurred by the limited lengths of upwind stencils of the baseline WENOCU4. The shock sensor gives low resolution for these regions. Such a phenomenon will vanish with improving order of the scheme (Zhao et al., 2019a). On the other hand, no misidentification is induced by the optimized WENOCU4 with the binary switch in the high-gradient smooth post-shock region while other switches will misidentify several smooth points where lower values of C are employed. Although these C values at the misidentified points are about one order of magnitude larger than $C_{\min}$, these two switches may achieve more misidentifications in the simulation of complex problems.

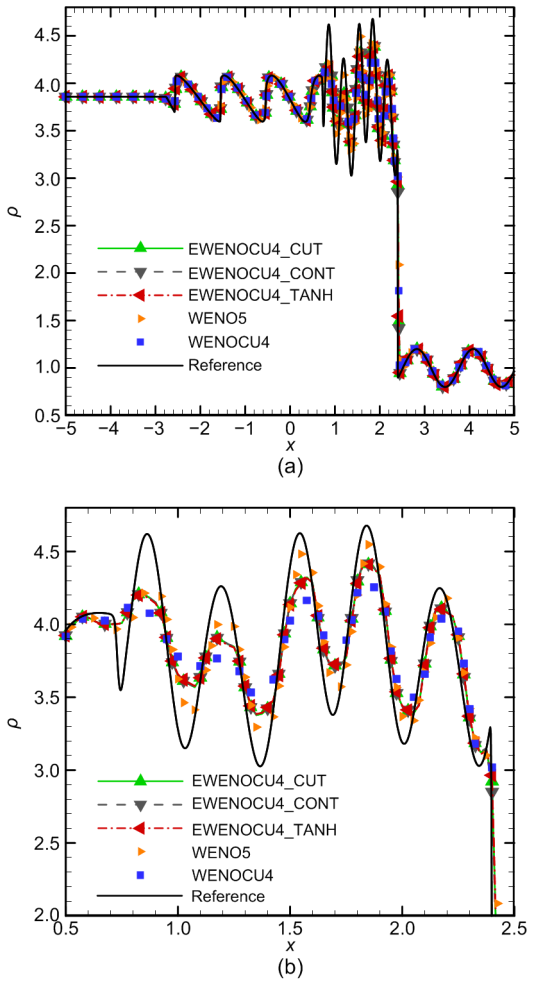

Fig. 16 Numerical solution of Shu-Osher problem obtained by different schemes with 400 cells
(a) Global view; (b) Local view

Generally, the results indicate the good capability of the EWENOCU4 scheme for resolving complex small-scale flow features and preserving the necessary dissipation for resolving shocks with moderate-to-strong intensity.

3.3 Applications to 2D Euler equations

Since the flow dynamics are driven by the inviscid Euler equations, no viscous dissipation is considered in the following benchmark cases. The

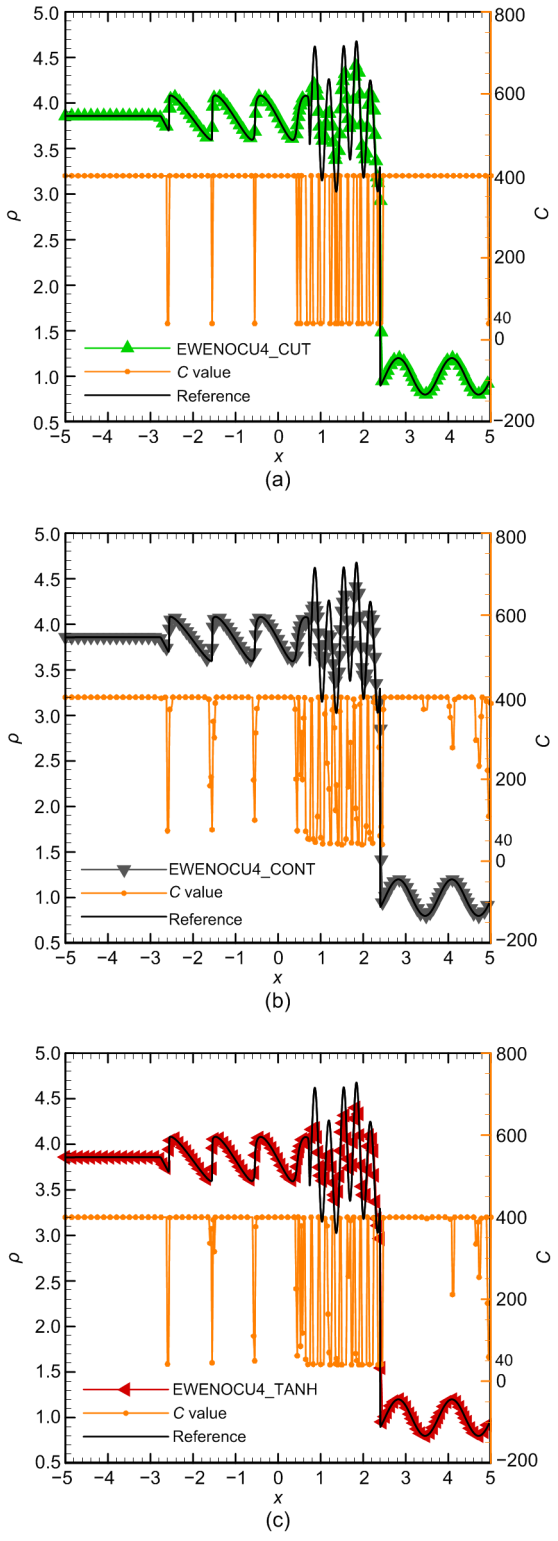

Fig. 17 Density and parameter *C* distributions of Shu-Osher problem computed by EWENOCU4 schemes with different switches using 400 cells

(a) EWENOCU4_CUT; (b) EWENOCU4_CONT; (c) EWENOCU4_TANH

discrete vortices around the contact discontinuities induced by Kelvin-Helmholtz instability are only damped by numerical dissipation. Less inherent numerical dissipation means more fine-scale rolled-up vortices can be resolved.

3.3.1 Riemann problem

For the test case suggested by Lax and Liu (1998), the Riemann initial conditions (non-dimensional density ρ, velocities v_x and v_y, and pressure p) are defined as:

$$(\rho, v_x, v_y, p)=\begin{cases}(1.5000, 0, 0, 1.500), \\ \qquad 0.8\le x\le 1,\ \ 0.8\le y\le 1, \\ (0.5323, 1.206, 0, 0.300), \\ \qquad 0\le x\le 0.8,\ \ 0.8\le y\le 1, \\ (0.1380, 1.206, 1.206, 0.029), \\ \qquad 0\le x\le 0.8,\ \ 0\le y\le 0.8, \\ (0.5323, 0, 1.206, 0.300), \\ \qquad 0.8\le x\le 1,\ \ 0\le y\le 0.8.\end{cases} \tag{31}$$

The computational domain is $x\in[0, 1]$ and $y\in[0, 1]$ with a resolution of 800×800 meshes. Initially, it involves the constant states of flow variables over each quadrant, obtained by dividing unit squares using lines x=0.8 and y=0.8. The boundaries are set as extrapolation boundary condition, that is the values are specified by the initial conditions at each quadrant, while the values of corresponding ghost points for each boundary change with time. The final simulation is t=0.8.

The solution of this case consists of a Mach stem and Kelvin-Helmholtz vortices along the slip lines originated at the triple points which result from a complex shock diffraction configuration. The complex discrete vortical structures in the mushroom-shaped jet can be regarded as an important criterion for evaluating the properties of schemes, especially in respect of their numerical robustness and dissipation.

Fig. 18 shows the density and parameter *C* profiles of schemes. At this mesh resolution, these schemes exhibit apparent differences in the jet wake. The WENO5 scheme can only capture the main flow features, including shocks, slip lines, and jet without any signature of Kelvin-Helmholtz vortices, because

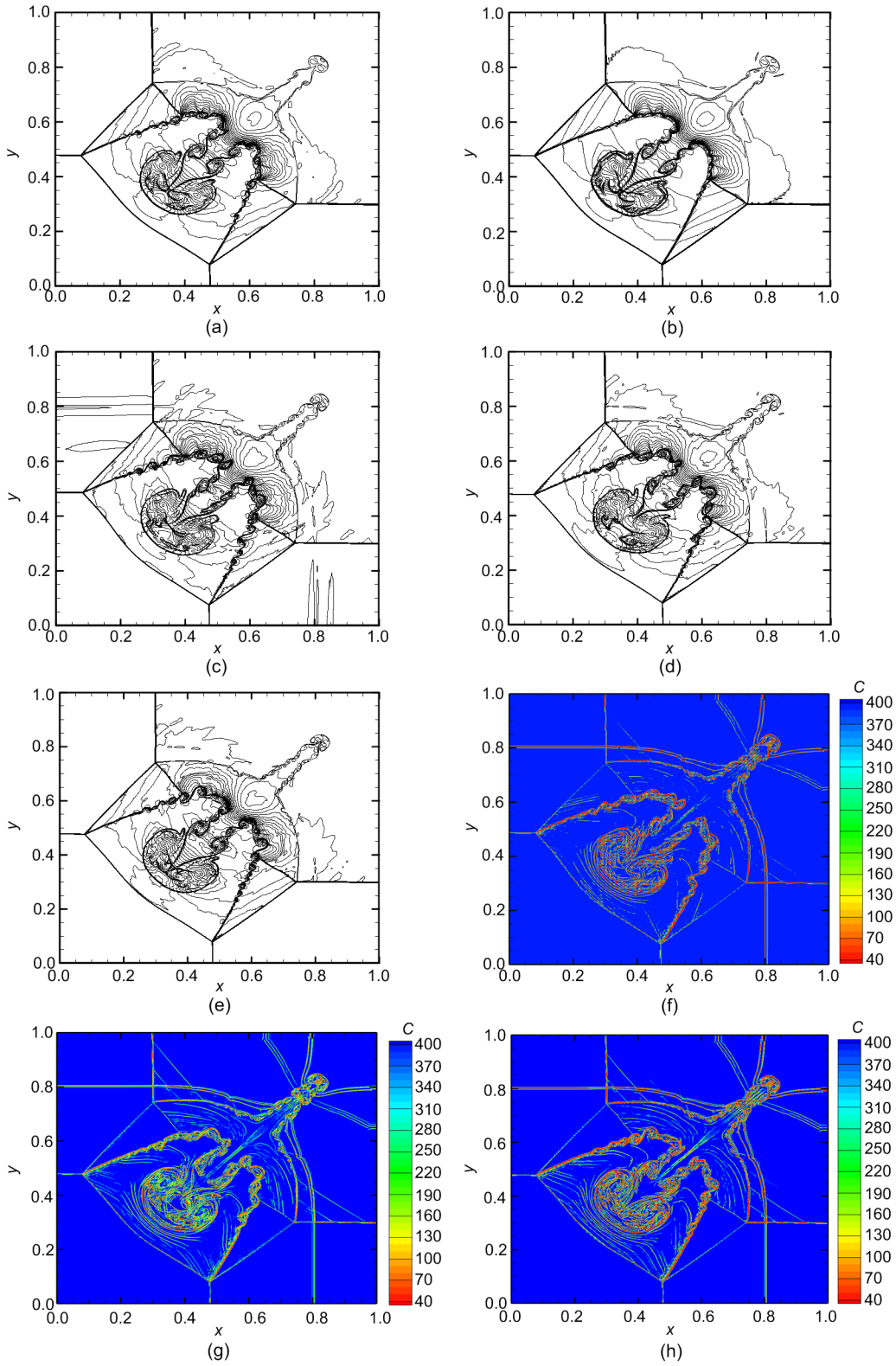

Fig. 18 Simulations of the 2D Riemann case for several shock-capturing schemes at t=0.8 on 800×800 meshes: (a)–(e) 33 equally spaced density contours from 0.2 to 1.8; (f)–(h) 13 equally spaced parameter C contours from 40 to 400

(a) WENOCU4; (b) WENO5; (c) EWENOCU4_CUT; (d) EWENOCU4_CONT; (e) EWENOCU4_TANH; (f) EWENOCU4_CUT, parameter C; (g) EWENOCU4_CONT, parameter C; (h) EWENOCU4_TANH, parameter C

of excessive numerical dissipation. More discrete vortices can be seen around the jet head regions for WENOCU4. It can be seen that EWENOCU4 achieves more superior solutions compared to other schemes. Specifically, abundant small-scale fluctuations can be resolved around the slip lines. It can be seen that EWENOCU4_CUT achieves a stable solution but also introduces a slight asymmetry of flow field, which is mainly due to the small numerical disturbance. As the discontinuities and discrete vortices are precisely perceived by the shock sensor and using adaptive parameter C, the inherent dissipation can be effectively restrained, which is why EWENOCU4 notably outperforms WENO5 and WENOCU4. On the other hand, the parameter C distributions accord with our analysis for the rationale of these three types of switches in Section 2.2. Generally, EWENOCU4_CUT shows a straightforward property: $C_{\min}$ is applied in discontinuities while $C_{\max}$ is applied in other regions. EWENOCU4_CONT exhibits an approximately linear transition from $C_{\min}$ to $C_{\max}$. Similarly, EWENOCU4_TANH also shows a smooth transition but in a "gentle" manner. Similar features can also be found from the following 2D benchmark cases.

3.3.2 Double-Mach reflection problem

The double-Mach reflection problem is a 2D inviscid canonical case (Woodward and Colella, 1984) for investigating the shock-capturing property and accuracy of the numerical algorithms. The richness of vertical structures along contact discontinuities illustrates the numerical viscosity of schemes. Initially, the boundary conditions are defined as

$$\left(\rho, v_x, v_y, p\right)=\begin{cases}\left(1.4, 0, 0, 1\right), & \\ & x>\dfrac{1}{6}+\dfrac{1}{\tan\dfrac{\pi}{3}}y,\\ \left(8, 7.145, -4.125, 116.8333\right), & \\ & \text{otherwise.}\end{cases} \tag{32}$$

The size of the computational domain is $x\in[0, 4]$ and $y\in[0, 1]$ with uniform 240×960 meshes. A right-moving 60°-inclined strong Ma=10 shock intersects the x-axis at x=1/6. The post-shock conditions are applied to the domain from the left boundary to the initial shock front except for part of the top boundary. The undisturbed air condition, that is ρ=1.4 and p=1, is applied to the domain ahead of the initial shock. The initial post-shock flow values are applied to the bottom boundary from x=0 to x=1/6 and the left boundary. The reflective condition is assigned from x=1/6 to x=4 along the bottom boundary. The values along the top boundary are set to describe the exact motion of the initial Ma=10 shock. The right boundary at x=4 is the outflow boundary and all the gradients are set to zero. The solution is advanced to t=0.2.

Fig. 19 depicts the enlarged views of triple points and slip lines for the density profile. The WENO5 scheme contains so much dissipation that hardly any small-scale vorticities can be produced. WENOCU4 resolves more vorticities around the contact lines, demonstrating that it introduces less numerical dissipation than WENO5. Especially, EWENOCU4 can give stable results and capture more rolled-up structures. It illustrates the obvious superiority of the adaptive parameter C. Moreover, it is clearly seen that there are no noticeable discrepancies among the results of these three different switches because only a specific shock sensor is used. We also plot the parameter C profile in Fig. 19. It can be observed that the locations of the massive fine-scale structures near the contact discontinuity employ smaller values of C, and the feature of C distribution accords with the rationale of these switches described in Section 2.2.

3.3.3 Rayleigh-Taylor instability problem

We consider the Rayleigh-Taylor instability problem (Young et al., 2001) to investigate the numerical properties of schemes. This case involves the instability between a heavy-density fluid and a light one.

The boundary conditions are initialized as

$$\left(\rho, v_x, v_y, p\right)=\begin{cases}\left(2, 0, -0.025c\cdot\cos\left(8\pi x\right), 2y+1\right), & \\ & 0\le y<0.5,\\ \left(1, 0, -0.025c\cdot\cos\left(8\pi x\right), y+1.5\right), & \\ & 0.5\le y\le 1,\end{cases} \tag{33}$$

where $c=\sqrt{\gamma(p/\rho)}$ denotes the sound speed and

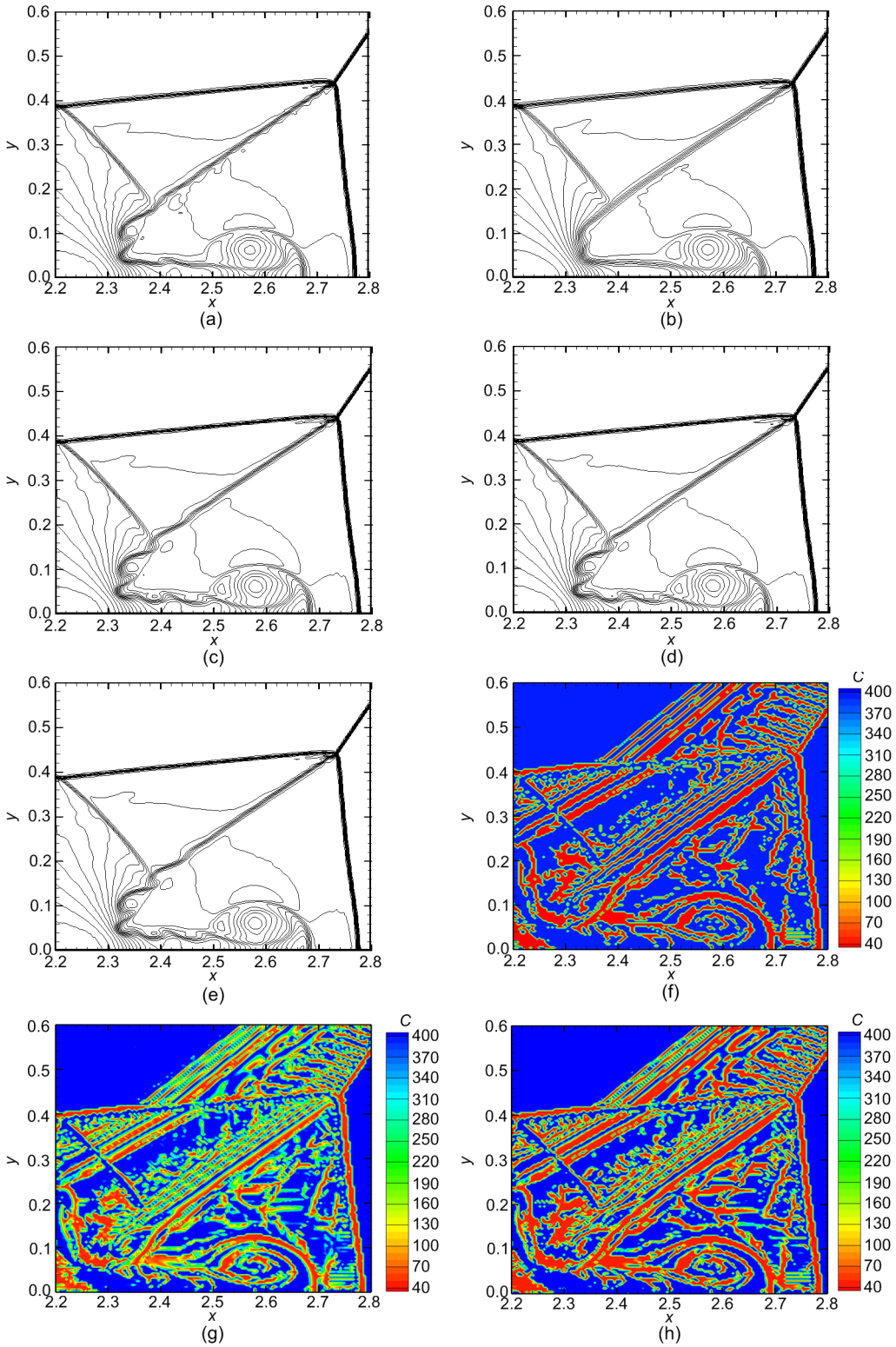

Fig. 19 Simulations of the double-Mach shock reflection problem for various shock-capturing schemes at t=0.2 on 240×960 meshes: (a)–(e) 36 equally spaced density contours from 2.2 to 19.7; (f)–(h) 13 equally spaced parameter C contours from 40 to 400

(a) WENOCU4; (b) WENO5; (c) EWENOCU4_CUT; (d) EWENOCU4_CONT; (e) EWENOCU4_TANH; (f) EWENOCU4_CUT, parameter C; (g) EWENOCU4_CONT, parameter C; (h) EWENOCU4_TANH, parameter C

γ=5/3. The computational domain is set as $x\in[0, 0.25]$ and $y\in[0, 1]$. The top and bottom boundaries are set as Dirichlet boundary conditions, that is at the bottom boundary, (ρ, v_x, v_y, p)=(2, 0, 0, 1) is assigned, and at the top boundary, (ρ, v_x, v_y, p)=(1, 0, 0, 2.5) is assigned. At the left and right boundaries, the reflective boundary conditions are used. For the flux reconstruction of the WENOCU4 scheme, two ghost points near the boundary are needed, and thus at the top and bottom boundaries, a general method is to set the same fixed values as the initial boundary conditions. The numerical solutions are advanced in time up to t=1.8. Since the inviscid Euler equations are solved here, the appearance of complex fine structures is related to the magnitude of numerical dissipation of the schemes.

Fig. 20 shows the density contours of simulations conducted on a uniform grid with 240×960 points. WENO5 cannot capture the detailed vortical structures, indicating its high-dissipation property. The result from WENOCU4 is much better than WENO5. Apparent improvements are obtained with the EWENOCU4 scheme, which gives considerable advantages over other schemes in resolving the refined discrete vortices in the shear layer regions. Moreover, the EWENOCU4 schemes with different switches give similar solutions except for a slight discrepancy. Only EWENOCU4_CONT induces a slight asymmetry structure, which is mainly due to slight numerical disturbances (Fleischmann et al., 2019). Furthermore, Fig. 21 shows the parameter C profile of the EWENOCU4 scheme. Similar to the features of the aforementioned 2D test cases, the roll-up of vortices and the small-scale flow structures in the shear layer regions are captured by the shock sensor and these complex structures are applied at smaller C values. Also, the features of C distribution conform to the analysis of these switches described in Section 2.2. Generally, the assessment for the Rayleigh-Taylor instability problem further confirms the low-dissipation superiority of the EWENOCU4 scheme in resolving small-scale vortical structures.

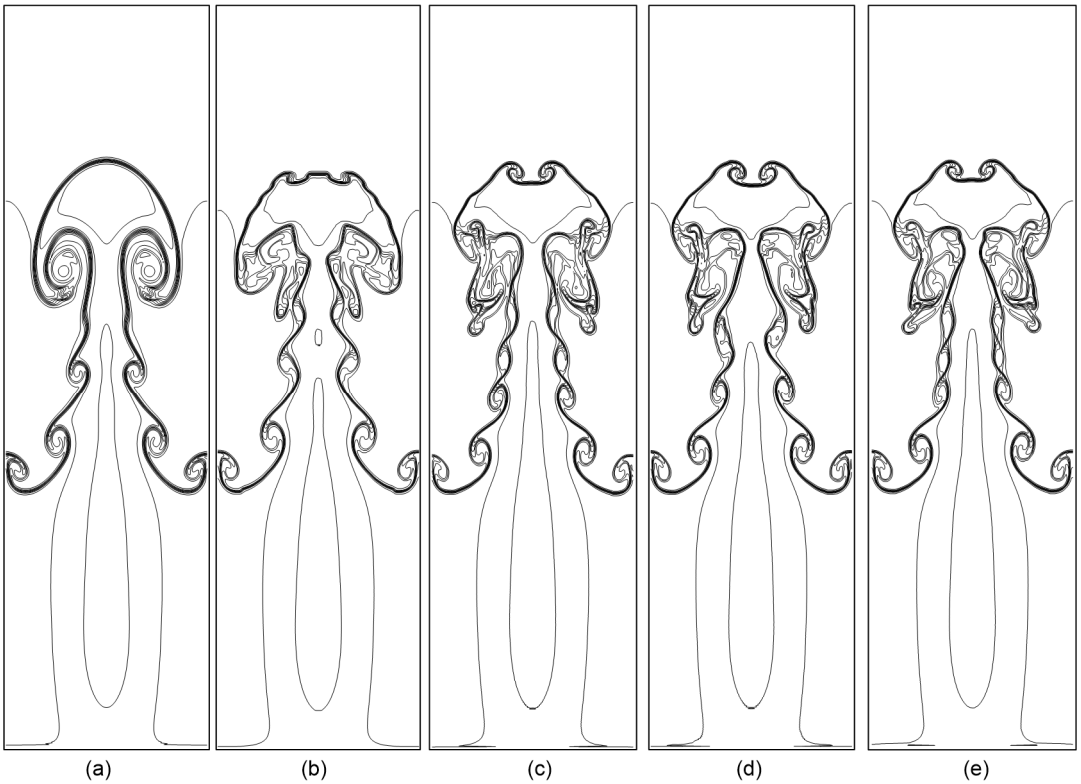

Fig. 20 Simulations of Rayleigh-Taylor instability problem for various shock-capturing schemes at t=1.8 on 240×960 meshes with 11 equally spaced density contours from 0.95 to 2.25
(a) WENO5; (b) WENOCU4; (c) EWENOCU4_CUT; (d) EWENOCU4_CONT; (e) EWENOCU4_TANH

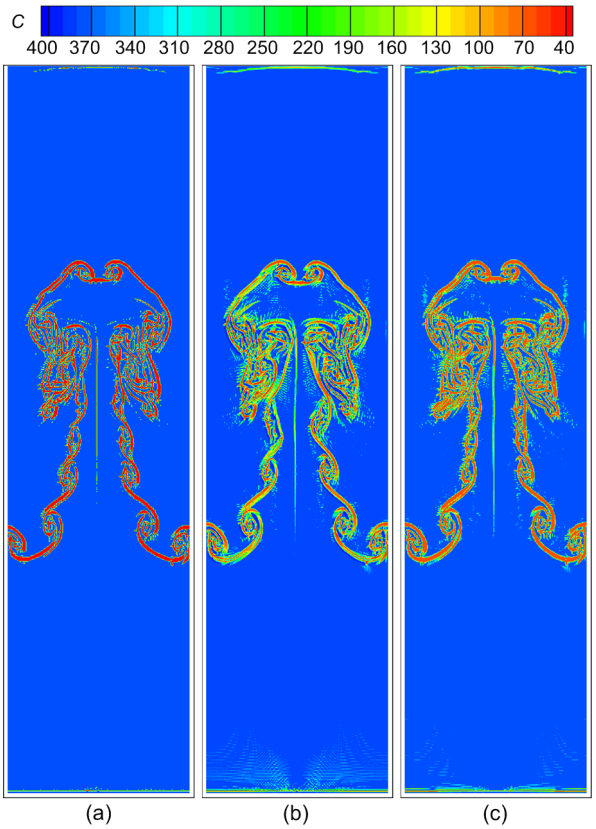

Fig. 21 Simulations of Rayleigh-Taylor instability problem for EWENOCU4 schemes with different switches at t=1.8 on 240×960 meshes with 13 equally spaced parameter C contours from 40 to 400

(a) EWENOCU4_CUT; (b) EWENOCU4_CONT; (c) EWENOCU4_TANH

3.4 Application to 3D Euler equations

Here, we consider the isotropic compressible turbulence case (Li et al., 2002) to evaluate the turbulence simulation capabilities of the schemes. The computational domain is a 2π×2π×2π cube that is computed on a grid with 64×64×64 points without viscosity involved. All boundaries are set as periodic boundary conditions. The initial random solenoidal velocity field $u_{i,0}$ satisfies:

$$\frac{3}{2}u_{\mathrm{rms},0}^2=\frac{\langle u_{i,0}^2\rangle}{2}=\int_0^\infty E(k^*)\mathrm{d}k^*, \tag{34}$$

$$E(k^*)=Ak^{*4}\mathrm{e}^{-2\left(\frac{k^*}{k_0^*}\right)^2}, \tag{35}$$

where $u_{\mathrm{rms}}=\sqrt{\langle u_i^2\rangle/3}$ is the root mean square of turbulent velocity field, k^* is the wavenumber, k_0^*=8 is the wavenumber at which the spectrum peaks, $E(k^*)$ is the energy spectrum, and A=0.00013 is the coefficient of the initial energy spectrum. The symbol $\langle\cdot\rangle$ denotes a volume average over the computational domain at a fixed time instant.

Initially, no fluctuations of any thermodynamic quantities (γ=1.4, density ρ_0=1.625, pressure p_0=4.643, and temperature T_0=1) are set, and the initial turbulence Mach number is $Ma_{\mathrm{t}0}=\sqrt{3}u_{\mathrm{rms},0}/\langle c_0\rangle=0.5$. The turbulence Mach number is given by $Ma_{\mathrm{t}}=\sqrt{\langle u_i^2\rangle}/\langle c\rangle$, where c denotes the local sound speed. The non-dimensional quantity k' is defined by $k'=\langle u_{\mathrm{rms}}^2\rangle/\langle c^2Ma_{\mathrm{t}0}^2\rangle$ (Honein and Moin, 2004). The time history of normalized average kinetic energy is defined as $K(t)/K_0$, where $K(t)=0.5\langle\rho u_i^2\rangle$ is the average turbulent kinetic energy, and $K_0=\frac{3A}{64}\sqrt{2\pi}k_0^{*5}$ is the initial average turbulent kinetic energy. t/τ denotes the normalized time, and $\tau=\sqrt{\frac{32}{A}}(2\pi)^{\frac{1}{4}}k_0^{*-\frac{7}{2}}$ is the large-eddy turnover time.

Fig. 22a depicts the non-dimensional fluctuation simulation results of schemes. All the fluctuation results attain a peak value after one large-eddy turnover time τ and decay afterward. The results of the EWENOCU4 schemes are noticeably better than those of WENOCU4 and WENO5. It can be observed that the fluctuation results of the optimized WENOCU4 with a continuous switch are slightly better than with other switches. However, the difference can be neglected.

Fig. 22b displays the time history of normalized average turbulent kinetic energy. As can be seen, the kinetic energies in all the schemes decay slowly with time evolution and finally reach equilibrium values. WENO5 decays the fastest, WENOCU4 moderately, and EWENOCU4 is the slowest. There is no obvious difference in the EWENOCU4 scheme with different switches.

Fig. 22c gives the energy spectra. As expected, EWENOCU4 achieves superior characteristics compared to the other schemes, demonstrating that employing adaptive switches can significantly improve the turbulence simulation ability compared with the original schemes. Also, the performance of these switches is similar.

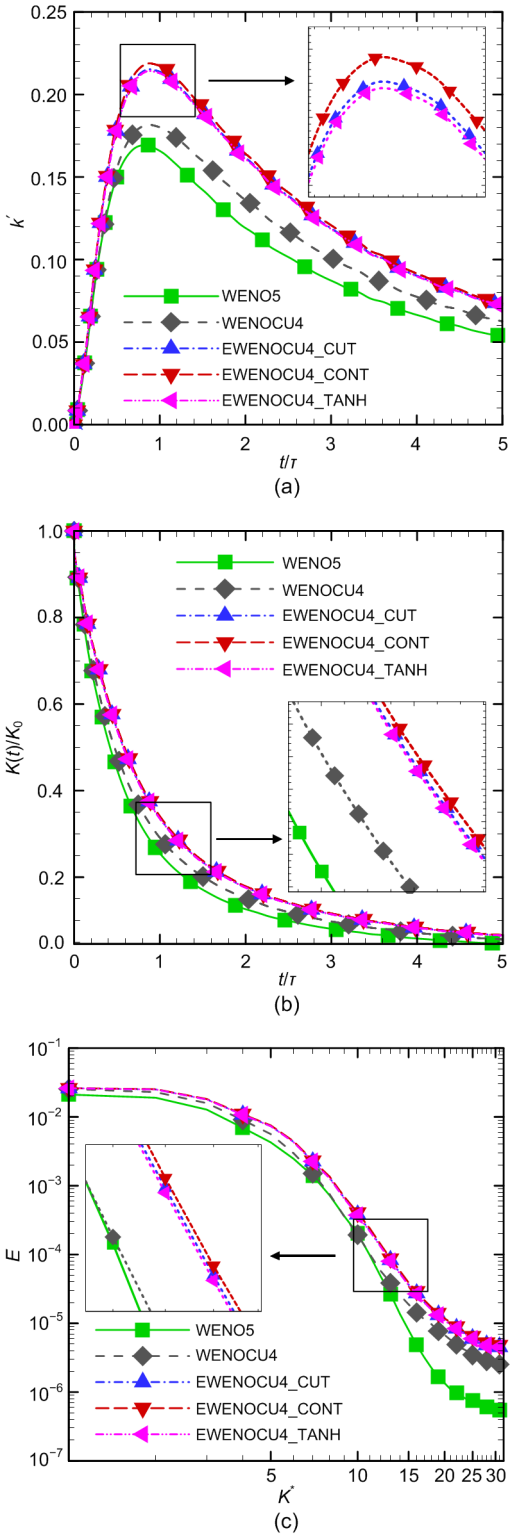

Fig. 22 Simulations of isotropic turbulence for various shock-capturing schemes at zero viscosity at Ma_{t0}=0.5
(a) Time history of the non-dimensional fluctuations; (b) Time evolution of the normalized average kinetic energy; (c) Energy spectrum

Fig. 23 presents the coherent randomly worm-like vortical structures identified by Q criteria (Jeong and Hussain, 1995) and colored by temperature at t=5τ. It can be observed that different schemes show remarkable differences in the number of vortices, with the notable outcome that the EWENOCU4 scheme has the lowest numerical dissipation. Similarly, there is no distinct difference among EWENOCU4 schemes with different switches.

4 Conclusions

This study provides the reference values of parameter C of WENOCU4 and systematically evaluates the comprehensive properties of three different adaptive switches for dynamically adjusting the parameter C. Numbers of numerical tests are analyzed, including 1D scalar equations, EDR analysis, and multi-dimensional Euler equations. The results illustrate that C=40 is a reasonable value for WENOCU4 rather than directly employing C=20 from WENOCU6. Moreover, numerical results further indicate that C_{max}=400 is a suitable value for the construction of switches. The method of employing adaptive parameters C_{min} (C_{min}=C) and C_{max} can efficiently overcome the inefficiency of using a constant small value. The optimized EWENOCU4 scheme with any type of adaptive switch exhibits considerable superiority compared with the original WENOCU4 and even higher-order WENO5 schemes, especially at 2D and 3D tests of Euler equations. For the case of 1D scalar equations, EWENOCU4 shows much less attenuation associated with propagation error in the post-shock smooth regions. In the wave-number space, EWENOCU4 exhibits higher-resolution spectral properties compared to the baseline scheme. As for the test cases of Euler equations, the results further confirm that sharp discontinuities can be accurately captured without evident misidentification and more highly fluctuating small-scale structures can be resolved by assigning the adaptive parameter C. Certainly, all the solutions maintain numerical stability and robustness. For the dispersion and dissipation properties of the three switches, there is no significant difference. Generally, the EWENOCU4 scheme with the binary switch shows superior performance compared with other switches.

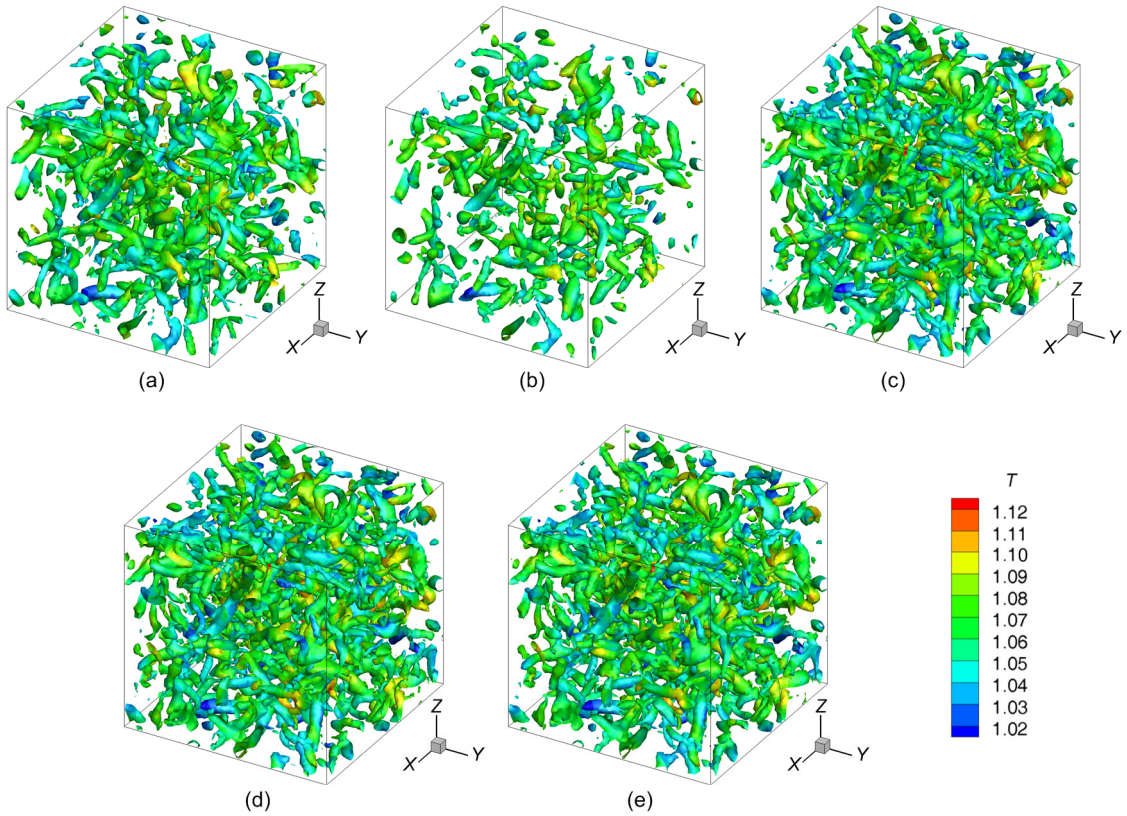

Fig. 23 Coherent randomly worm-like vortical structures identified by Q=0.5 criteria and colored by temperature T for various shock-capturing schemes

(a) WENOCU4; (b) WENO5; (c) EWENOCU4_CUT; (d) EWENOCU4_CONT; (e) EWENOCU4_TANH

Firstly, the binary switch can filter several misidentifications in smooth regions compared with others, especially in the model sound wave refraction and shock-entropy wave interaction cases. Moreover, the computational efficiency of the binary switch is superior to that of the hyperbolic tangent switch. Therefore, employing the binary switch is a more cost-effective choice for numerical schemes for simultaneously restraining the numerical dissipation and resolving broadband fluctuations.

This study provides useful guidance for the reference values of adaptive C and the evaluation of adaptive switches. It needs to be pointed out that, although the evaluations for these switches are obtained based on a particular scheme, namely WENOCU4, the results have general validity. Therefore, the cost-effective binary switch is recommended for application to other WENO schemes, especially the ones based on WENOCU schemes. As a final remark, we should point out that, especially in 1D problems previously presented, the parameter C may change into $C_{\max}$ near several discontinuities that are misidentified as continuous points. As we know, improving the resolution is at the expense of incurring more oscillatory solutions. This raises the fundamental issue of when a flow region should be actually perceived as a "discontinuity." This is of course far from being satisfactory from a theoretical standpoint, and additional research is probably appropriate to tackle this long-standing fundamental issue.

Contributors

Liang LI and Guo-yan ZHAO designed the methodology conception and realized the programming. Da-peng XIONG and Tao TANG processed the corresponding data. Liang LI, Guo-yan ZHAO, and Hong-bo WANG performed formal analysis and investigation. Liang LI wrote the first draft of the manuscript. Guo-yan ZHAO, Hong-bo WANG, and Ming-bo SUN revised and edited the final version.

Conflict of interest

Liang LI, Hong-bo WANG, Guo-yan ZHAO, Ming-bo SUN, Da-peng XIONG, and Tao TANG declare that they have no conflict of interest.

References

Adams NA, Shariff K, 1996. A high-resolution hybrid compact-ENO scheme for shock-turbulence interaction problems. *Journal of Computational Physics*, 127(1):27-51. https://doi.org/10.1006/jcph.1996.0156

Borges R, Carmona M, Costa B, et al., 2008. An improved weighted essentially non-oscillatory scheme for hyperbolic conservation laws. *Journal of Computational Physics*, 227(6):3191-3211. https://doi.org/10.1016/j.jcp.2007.11.038

Casper J, Carpenter MH, 1998. Computational considerations for the simulation of shock-induced sound. *SIAM Journal on Scientific Computing*, 19(3):813-828. https://doi.org/10.1137/s1064827595294101

Fleischmann N, Adami S, Adams NA, 2019. Numerical symmetry-preserving techniques for low-dissipation shock-capturing schemes. *Computers & Fluids*, 189:94-107. https://doi.org/10.1016/j.compfluid.2019.04.004

Henrick AK, Aslam TD, Powers JM, 2005. Mapped weighted essentially non-oscillatory schemes: achieving optimal order near critical points. *Journal of Computational Physics*, 207(2):542-567. https://doi.org/10.1016/j.jcp.2005.01.023

Honein AE, Moin P, 2004. Higher entropy conservation and numerical stability of compressible turbulence simulations. *Journal of Computational Physics*, 201(2):531-545. https://doi.org/10.1016/j.jcp.2004.06.006

Hu XY, Wang Q, Adams NA, 2010. An adaptive central-upwind weighted essentially non-oscillatory scheme. *Journal of Computational Physics*, 229(23):8952-8965. https://doi.org/10.1016/j.jcp.2010.08.019

Hu XY, Wang B, Adams NA, 2015. An efficient low-dissipation hybrid weighted essentially non-oscillatory scheme. *Journal of Computational Physics*, 301:415-424. https://doi.org/10.1016/j.jcp.2015.08.043

Jeong J, Hussain F, 1995. On the identification of a vortex. *Journal of Fluid Mechanics*, 285:69-94. https://doi.org/10.1017/S0022112095000462

Jiang GS, Shu CW, 1996. Efficient implementation of weighted ENO schemes. *Journal of Computational Physics*, 126(1):202-228. https://doi.org/10.1006/jcph.1996.0130

Larsson J, Gustafsson B, 2008. Stability criteria for hybrid difference methods. *Journal of Computational Physics*, 227(5):2886-2898. https://doi.org/10.1016/j.jcp.2007.11.025

Lax PD, 1954. Weak solutions of nonlinear hyperbolic equations and their numerical computation. *Communications on Pure and Applied Mathematics*, 7(1):159-193. https://doi.org/10.1002/cpa.3160070112

Lax PD, Liu XD, 1998. Solution of two-dimensional Riemann problems of gas dynamics by positive schemes. *SIAM Journal on Scientific Computing*, 19(2):319-340. https://doi.org/10.1137/S1064827595291819

Lele SK, 1992. Compact finite difference schemes with spectral-like resolution. *Journal of Computational Physics*, 103(1):16-42. https://doi.org/10.1016/0021-9991(92)90324-R

Li XL, Fu DX, Ma YW, 2002. Direct numerical simulation of compressible isotropic turbulence. *Science in China Series A: Mathematics*, 45(11):1452-1460. https://doi.org/10.1007/BF02880040

Liu XD, Osher S, Chan T, 1994. Weighted essentially non-oscillatory schemes. *Journal of Computational Physics*, 115(1):200-212. https://doi.org/10.1006/jcph.1994.1187

Martín MP, Taylor EM, Wu M, et al., 2006. A bandwidth-optimized WENO scheme for the effective direct numerical simulation of compressible turbulence. *Journal of Computational Physics*, 220(1):270-289. https://doi.org/10.1016/j.jcp.2006.05.009

Pirozzoli S, 2002. Conservative hybrid compact-WENO schemes for shock-turbulence interaction. *Journal of Computational Physics*, 178(1):81-117. https://doi.org/10.1006/jcph.2002.7021

Pirozzoli S, 2006. On the spectral properties of shock-capturing schemes. *Journal of Computational Physics*, 219(2):489-497. https://doi.org/10.1016/j.jcp.2006.07.009

Pirozzoli S, 2011. Numerical methods for high-speed flows. *Annual Review of Fluid Mechanics*, 43:163-194. https://doi.org/10.1146/annurev-fluid-122109-160718

Sod GA, 1978. A survey of several finite difference methods for systems of nonlinear hyperbolic conservation laws. *Journal of Computational Physics*, 27(1):1-31. https://doi.org/10.1016/0021-9991(78)90023-2

Taylor EM, Wu MW, Martín MP, 2007. Optimization of nonlinear error for weighted essentially non-oscillatory methods in direct numerical simulations of compressible turbulence. *Journal of Computational Physics*, 223(1):384-397. https://doi.org/10.1016/j.jcp.2006.09.010

Woodward P, Colella P, 1984. The numerical simulation of two-dimensional fluid flow with strong shocks. *Journal of Computational Physics*, 54(1):115-173. https://doi.org/10.1016/0021-9991(84)90142-6

Wu XS, Zhao YX, 2015. A high-resolution hybrid scheme for hyperbolic conservation laws. *International Journal for Numerical Methods in Fluids*, 78(3):162-187. https://doi.org/10.1002/fld.4014

Young YN, Tufo H, Dubey A, et al., 2001. On the miscible Rayleigh-Taylor instability: two and three dimensions. *Journal of Fluid Mechanics*, 447:377-408. https://doi.org/10.1017/S0022112001005870

Zhao GY, Sun MB, Mei Y, et al., 2019a. An efficient adaptive central-upwind WENO-CU6 numerical scheme with a new sensor. *Journal of Scientific Computing*, 81(2):649-670. https://doi.org/10.1007/s10915-019-01035-9

Zhao GY, Sun MB, Memmolo A, et al., 2019b. A general framework for the evaluation of shock-capturing schemes. *Journal of Computational Physics*, 376:924-936. https://doi.org/10.1016/j.jcp.2018.10.013

Zhao GY, Sun MB, Pirozzoli S, 2020. On shock sensors for hybrid compact/WENO schemes. *Computers & Fluids*, 199:104439. https://doi.org/10.1016/j.compfluid.2020.104439

中文概要

题　目: 三种不同自适应开关的高效 WENOCU4 格式研究

目　的: 现有研究尚未提供 WENOCU4 格式中参数 C 的建议值。本文旨在根据流场特性自适应地调节参数 C 的量级从而提高格式的数值表现。为此，通过广泛的数值模拟以提供自适应参数 C 的参考值，并系统地评估三种能够自适应调节参数 C 的开关的性能，测得综合表现最佳的开关，进而为获得高阶 WENO 改进型格式提供参考。

创新点: 1. 提供了高效 WENOCU4 格式的自适应参数 C 的参考值；2. 系统地评估了三种自适应开关（二进制型、连续型和双曲正切型）的性能，并证实了二进制型开关的最佳表现。

方　法: 1. 通过理论分析，系统研究三种自适应开关的原理和性能特点；2. 通过广泛的数值模拟（包括一维标量方程、经验色散关系和多维欧拉方程的标准算例），获得自适应参数 C 的参考值并验证其合理性；3. 通过广泛的数值模拟，系统评估三种自适应开关的综合表现（包括数值色散和耗散特性以及计算效率），并获得综合性能最佳的自适应开关。

结　论: 1. 对于高效 WENOCU4 格式而言，本研究证实了 C_{min}=40 和 C_{max}=400 是合理的自适应参数 C 的参考值，因此不应该直接采用 WENOCU6 的原始建议值。2. 根据流场的连续性，采用自适应的参数 C 可以在保证数值稳定性的同时，有效地抑制 WENOCU4 的数值耗散。3. 相比于其它开关，二进制型开关的综合表现最佳；其能够过滤激波感知器在光滑区域的一些误判，构造简单，且计算效率较高。4. 本研究对三种自适应开关的评估具有一般性，因此易于拓展到其它高阶 WENO 格式的改进工作中。

关键词: WENOCU4；激波捕捉格式；自适应开关；数值鲁棒性；耗散性